

Cystatin A, a Potential Common Link for Mutant Myocilin Causative Glaucoma

K. David Kennedy, S. A. AnithaChristy, LaKisha K. Buie, Teresa Borrás*

Department of Ophthalmology, University of North Carolina School of Medicine, Chapel Hill, North Carolina, United States of America

Abstract

Myocilin (MYOC) is a 504 aa secreted glycoprotein induced by stress factors in the trabecular meshwork tissue of the eye, where it was discovered. Mutations in *MYOC* are linked to glaucoma. The glaucoma phenotype of each of the different *MYOC* mutation varies, but all of them cause elevated intraocular pressure (IOP). In cells, forty percent of wild-type MYOC is cleaved by calpain II, a cysteine protease. This proteolytic process is inhibited by MYOC mutants. In this study, we investigated the molecular mechanisms by which MYOC mutants cause glaucoma. We constructed adenoviral vectors with variants Q368X, R342K, D380N, K423E, and overexpressed them in human trabecular meshwork cells. We analyzed expression profiles with Affymetrix U133Plus2 GeneChips using wild-type and null viruses as controls. Analysis of trabecular meshwork relevant mechanisms showed that the unfolded protein response (UPR) was the most affected. Search for individual candidate genes revealed that genes that have been historically connected to trabecular meshwork physiology and pathology were altered by the *MYOC* mutants. Some of those had known *MYOC* associations (*MMP1*, *PDIA4*, *CALR*, *SFPR1*) while others did not (*EDN1*, *MGP*, *IGF1*, *TAC1*). Some, were top-changed in only one mutant (*LOXL1*, *CYP11B1*, *FBN1*), others followed a mutant group pattern. Some of the genes were new (*RAB39B*, *STC1*, *CXCL12*, *CSTA*). In particular, one selected gene, the cysteine protease inhibitor cystatin A (*CSTA*), was commonly induced by all mutants and not by the wild-type. Subsequent functional analysis of the selected gene showed that *CSTA* was able to reduce wild-type MYOC cleavage in primary trabecular meshwork cells while an inactive mutated *CSTA* was not. These findings provide a new molecular understanding of the mechanisms of MYOC-causative glaucoma and reveal *CSTA*, a serum biomarker for cancer, as a potential biomarker and drug for the treatment of MYOC-induced glaucoma.

Citation: Kennedy KD, AnithaChristy SA, Buie LK, Borrás T (2012) Cystatin A, a Potential Common Link for Mutant Myocilin Causative Glaucoma. PLoS ONE 7(5): e36301. doi:10.1371/journal.pone.0036301

Editor: Reiner Albert Veitia, Institut Jacques Monod, France

Received: November 11, 2011; **Accepted:** April 4, 2012; **Published:** May 15, 2012

Copyright: © 2012 Kennedy et al. This is an open-access article distributed under the terms of the Creative Commons Attribution License, which permits unrestricted use, distribution, and reproduction in any medium, provided the original author and source are credited.

Funding: This work was supported by National Institutes of Health (USA) grants EY11906 (TB), EY13126 (TB), EY015873 (RHHA), and by a Research to Prevent Blindness unrestricted grant to the UNC Department of Ophthalmology. The funders had no role in study design, data collection and analysis, decision to publish, or preparation of the manuscript.

Competing Interests: The authors have declared that no competing interests exist.

* E-mail: tborras@med.unc.edu

Introduction

The secreted glycoprotein, myocilin (MYOC), was identified in human trabecular meshwork (HTM) cells after prolonged exposure to dexamethasone (DEX) (*Trabecular Meshwork Inducible protein*, *TIGR*) [1]. It was independently discovered in the ciliary body [2] and in the normal retina [3]. The gene was later found to be expressed in non-ocular tissues, especially in heart and skeletal muscle [4]. However, MYOC retained special properties in the trabecular meshwork and its induction by DEX is specific to this tissue [5]. Soon after its discovery, mutations in the *MYOC* gene were found to be linked to 3–4% of primary open-angle glaucoma (POAG) [6] and to a large percent (10–30%) to juvenile open-angle glaucoma (JOAG), an early-onset and more severe form of the disease [7].

The glaucomas are a group of optic neuropathies caused by the degeneration and death of the retinal ganglion cells. In glaucoma, there is a progressive visual field loss and if left untreated, it leads to irreversible blindness. It is estimated that by 2020 there will be 79.6 million cases of glaucoma worldwide, with a high proportion of women and Asians [8]. POAG is the most common form of the disease, which in most cases, is triggered by an elevated intraocular pressure (IOP). In turn, elevated IOP is the result of an increased

resistance of the trabecular meshwork tissue to the aqueous humor outflow.

To date, more than 70 *MYOC* mutations have been associated with glaucoma (<http://myocilin.com/>) [9]. Each of the mutations results in a slightly different phenotype, it is more prevalent in a given race and some have been speculated to be affected by environmental epigenetic factors (reviewed in [9]). Nevertheless, in every case, mutations in *MYOC* are associated with elevated IOP, ranging from mild to severe (<http://myocilin.com/>). Because of the relevance of this association, the MYOC protein has been extensively studied.

Myocilin is a 504 amino acid protein with a molecular weight of 55–57 kDa [10,11]. The gene maps to 1q23–q24 [6] and contains three exons, which pretty much define three protein folding domains [4,10]. The N-domain (aa 1 to 202) contains a signal peptide cleavage, a leucine zipper-like motif and is similar to the heavy chain of myosin [4,10]. The C-terminal domain (aa 244 to 505), separated by a central linker (aa 203 to 205), is 40% homologous to olfactomedin, a major component of the extracellular matrix (ECM) of the olfactory neuroepithelium. The original finding that *MYOC* mutants mapped to the olfactomedin domain has held, and today, over 90% percent of pathogenic mutations

are known to occur in that third exon of the protein (<http://myocilin.com/>).

Although considerable progress has been made, many questions regarding the function of wild-type MYOC and the molecular correlations of the different mutant variants to disease severity remain. Myocilin is processed and shed inside vesicles [12,13]. In contrast to the wild-type, recombinant mutants in the olfactomedin domain, whether generic, glaucoma-associated, stop or missense, are unable to exit the cell in all cell types tried [5,12,14,15]. Our earlier work also showed that mutant MYOC proteins lacking the olfactomedin domain are misfolded, form insoluble aggregates and accumulate in the endoplasmic reticulum (ER) [11]. Further, presence of increasing amounts of the recombinant mutant induces a fraction of the soluble, wild-type MYOC to move to the insoluble fraction and hamper its secretion [11]. Glaucoma-associated mutants are likewise insoluble [16] and hetero-oligomers with the wild-type are sequestered in the ER [17], leading to ER stress, activation of the unfolded protein response (UPR) and potential cytotoxicity [18,19]. This data, supported by clinical findings on the absence of POAG in homozygous patients for certain MYOC mutants [20] led to the conclusion that MYOC-linked glaucoma was due to a gain of function.

In addition to glucocorticoids, *MYOC* expression is induced by a number of stress factors. Mechanical stretch, TGF- β , oxidative stress, heat shock and elevated IOP all induce *MYOC* in cells and tissues (review in [21,22]). In addition, expression of *MYOC* mutants sensitizes cells to oxidative stress [23]. Myocilin interacts with several intracellular and extracellular matrix proteins (review in [24]). Recently it was shown to interact with components of the WNT signaling pathway [25], which was independently found to be associated to regulation of IOP [22,26].

In the ER, MYOC undergoes an intracellular endoproteolytic cleavage in the central linker domain [27,28]. This processing occurs in ~40% of the wild-type protein and yields a 35 kDa fragment which is co-secreted with the full-length [28]. Myocilin mutants inhibit the proteolytic processing and the extent of inhibition has been correlated with the severity of the glaucoma phenotypes [28]. In addition, this proteolytic process modulates the molecular interactions of myocilin and reduces the formation of myocilin homoaggregates [29]. The enzyme responsible for this cleavage has been identified as Calpain II [30], a calcium-dependent cysteine protease present in most mammalian tissues.

All these findings put together reveal the potential involvement of many different genes in the functions leading to the *MYOC*-linked glaucoma. Previously, we reported a first microarray analysis using wild-type *MYOC* and high density oligonucleotide Affymetrix U133A GeneChips [31]. To now identify molecular differences among the effects of the causative glaucoma *MYOC* mutants, in this study we conducted an expression analysis on the transcriptome of primary human trabecular meshwork cells overexpressing *MYOC* mutants, and performed the analysis using the upgraded Affymetrix U133 Plus 2.0 GeneChips. We selected four representative mutants, based on different clinical outcomes, populations and/or relevance of the mutated codon. The Q368X variant is the most common (29% of the diseased causing variants) and results in a mild phenotype (<http://myocilin.com/>). Mutations R342K and D380N comprise 0.8% of the causing variants each, and are very severe, with a mean maximum IOP of 54 and 39 mmHg [32]. Both mutations have been reported only in one population, that of Ghana in West Africa. However while there is only one variant utilizing amino acid Arg342, the amino acid Asp380, highly conserved in all vertebrates, has produced four disease causing variants (D380N, D380H, D380A, D380G) [9], a

recurrence known to occur very rarely in genetics. These four variants appear in different populations and in particular, the His and Ala changes result in intermediate glaucoma phenotypes and biochemical protein effects [15,28,33]. The last mutation, K423E, was selected because it occurs in two unrelated Caucasian populations [20,34], has a severe clinical outcome and exhibits the interesting feature that homozygous patients do not manifest the disease [20]. A similar analysis recently published utilized transgenic flies and analyzed changes in the transcriptome of 2–3 day old insects' whole heads [19].

Cystatin A (CSTA) is a member of the cystatin superfamily of proteins, some of which are active cysteine protease inhibitors, such as cystatin A (review in [35]). Within the cystatin superfamily, CSTA is characterized as a stefin [36]. Proteins of the stefin family, lack carbohydrates and disulfide bonds and have a molecular weight ~11 kDa. This single chain protein forms tight complexes and inhibits the activity of papain-type proteases, cathepsin B, H and L [36], and presumably other intracellular cysteine protease inhibitors. The short N-terminal region of CSTA, and in particular the evolutionary conserved Gly-4 residue has been shown to play a key role in the binding of the CSTA inhibitor to the target proteases, papain, cathepsin B and L [37]. Mutations of Gly-4 to aminoacids with longer side chains like arginine were also shown to be more deleterious for the binding that mutations to alanine or serine which have small side chains [37]. Cystatin A is present in various tissues (epidermis, polymorphonuclear granulocytes, liver and spleen) and has also been found in extracellular fluids [35]. A loss of function mutation for CSTA was recently linked to two families of Middle Eastern origin exhibiting exfoliative ichthyosis, a scaly skin disease [38]. Cystatin A is a known myoepithelial cell marker and its downregulation plays a role in carcinogenesis, from breast to brain tumors [35]. It is believed that CSTA regulates cellular proliferation, tumor growth and metastasis. Cystatin A expression is a negative prognostic marker in breast tumors of lymph node negative patients [35]. Recently, levels of CSTA in serum, together with manganese superoxide dismutase and MMP2, were shown to be reliable biomarkers for the detection of nasopharyngeal carcinomas patients [39].

In the present study, we searched for genes and mechanisms affected by overexpression of four myocilin mutants in primary human trabecular meshwork cells. Using microarray profiles, we found that the myocilin mutants altered a high number of genes which had been previously associated with trabecular meshwork physiological and glaucomatous conditions. Some genes were shared by all mutants while some were mutant-specific. The extracellular matrix gene ontology (GO) category was the most enriched and most significant. Of the four most common mechanisms, genes in the UPR list were changed the most. More important, this study uncovered cystatin A, a cysteine protein inhibitor induced by all mutants, which reduced the processing of wild-type myocilin in vitro. These findings provide a molecular insight into mechanisms that trigger MYOC-glaucoma and raise the possibility of using silencing or inhibition of *CSTA* as a potential treatment of the MYOC-mutant development of glaucoma.

Materials and Methods

Generation of Adenoviruses Carrying Wild-type and MYOC Glaucoma-associated Mutants

Plasmids carrying point mutations corresponding to four human *MYOC* mutations genetically linked to glaucoma were generated by site-directed mutagenesis using as a template clone pMC2 [11]

and the QuickChange mutagenesis kit (Stratagene, La Jolla, CA) [19]. The plasmids contained the MYOC mutations Q368X, R342K, D380N, and K423E (Figure 1). All mutant clones were re-amplified with 5'-*KpnI*-3'-*BamHI* ended primers to remove the *PmeI* site (*MYOC* nucleotides (nt) 4–1566) (all *MYOC* nt numbering is from access number AF001620) and subcloned into pCR2.1 (Invitrogen, Carlsbad, CA) for confirmation of sequence and presence of the mutations (clones pGL6, pGL9, pAC10, pAC14). *KpnI*-*NotI* restricted mutant cDNA fragments (1,596 nucleotides) were gel purified and inserted into pShuttle-CMV (generously donated by B. Vogelstein [40] for the generation of the recombinant adenoviral plasmid vectors (pGL7, pGL10, pAC11, pAC15). For the wild-type, the pKM1 plasmid (see below) was digested with *KpnI*-*NotI* and the isolated fragment inserted into the same pShuttle-CMV vector to yield pAC18 (total insert 1,601 bp containing 46 bp 5' and 33 bp 3' plasmid sequences flanking the 1,522 *MYOC* wild-type coding region).

The shuttle vectors were then linearized with *PmeI* and electroporated into BJ5183-Ad1 cells for homologous recombination with an adenovirus backbone plasmid using the AdEasy Adenoviral Vector System (Stratagene) following manufacturer's recommendations. The resultant Ad plasmid vectors (pGL8, pGL11, pAC12, pAC16, pAC19) were linearized with *PacI* and calcium phosphate-transfected (Clontech, Mountain View, CA) into early passages QBI-Human Embryonic Kidney (HEK) 293A cells (Qbiogene, Montreal, Quebec, Canada) for the production of the adenoviral recombinants (Adh.Q368X, Adh.R342K, Adh.D380N, Adh.K423E and Adh.MYOCWT). These viruses therefore carry each of the four *MYOC* mutants driven by the same CMV promoter. High titer stocks were obtained by propagation in

the same QBI-HEK 293A cells and purification by double binding CsCl density centrifugation as described [41]. A control virus carrying the same promoter and no transgene (Ad5.CMV-Null) was purchased from Qbiogene (Montreal, Canada) and grown and purified in our laboratory. For Adh.Q368X, the virus particle number was determined by measurement of its optical density at 260 nm using the formula $1 \mu\text{g of DNA} = 2.2 \times 10^{10}$ particles. For the remaining recombinants, physical particles were titrated as viral genomes (vg)/ml as described [41] using a *MYOC* fluorescent TaqMan primers/probe Hs00165345_m1 (Applied Biosystems, ABI, Foster City, CA) and the *MYOC* plasmid pAC12 for the generation of the standard curve. Viral infectivity (infectious units [IFU]/ml) was measured with a rapid titer kit (AdenoX; Clontech) also as described [41]. Viral lots used in these studies had concentrations between 2×10^{11} and 1×10^{12} vg/ml with infectivity values between 2×10^9 and 5×10^{10} IFU/ml. A second set of viral stocks were grown at the University of North Carolina Vector Core facility. All viral stocks used in the experiments were checked for the overexpression of *MYOC* mRNA by TaqMan PCR (probe Hs00165345_m1) and MYOC protein by western blot (goat anti-human polyclonal, Santa Cruz Biotechnology #21243, Santa Cruz, CA)).

Primary Culture of Human Trabecular Meshwork Cells

Primary human trabecular meshwork (HTM) HTM-72 and HTM-137 cell lines were generated respectively from the trabecular meshworks dissected from residual cornea rims of 29 and 39 years old donors (North Carolina Eye Bank) after surgical corneal transplants at the University of North Carolina Eye Clinic. The tissue was cut into small pieces, carefully attached to the

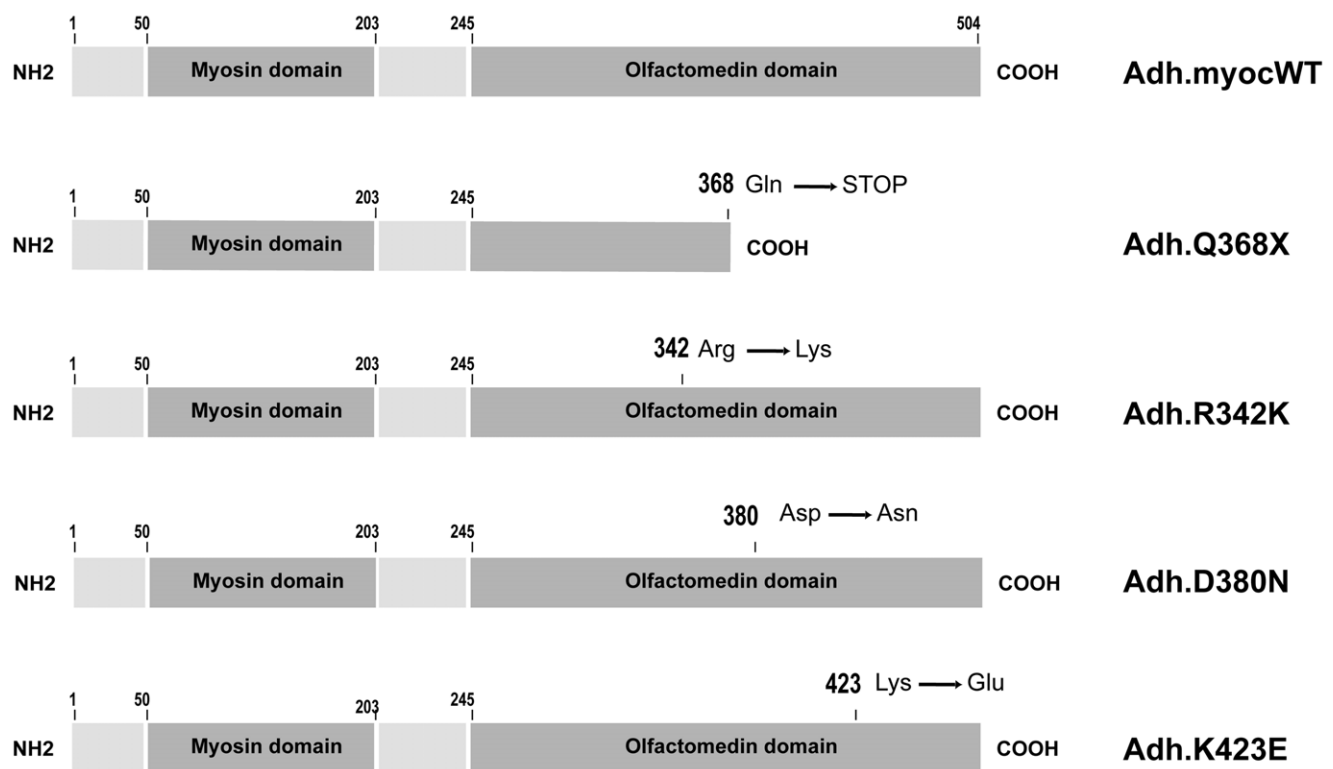


Figure 1. Schematic representation of MYOC wild-type and mutant proteins used for the adenoviral constructions. Myocilin protein contains a signal peptide cleavage (aa 1–50) and three folding domains. An N-terminal myosin domain (aa 50–203), a linker region (aa 203–245), and C-terminal olfactomedin domain (aa 245–504). All four selected mutants have mutations in the C-terminal olfaction domain. The Q368X mutation produces a truncated protein.

doi:10.1371/journal.pone.0036301.g001

bottom of the 2% gelatin-coated 35 mm dish, and covered slipped with a drop of MEM Richter's Modification medium (IMEM, HyClone, Thermo Fisher Scientific, Waltham, MA) supplemented with 20% heat-inactivated fetal bovine serum (FBS, GIBCO catalog # 16140-071), 50 µg/ml gentamicin (Invitrogen). Cells from these specimens were not treated with enzymes and were allowed to grow from the explant for a period of 4 weeks changing the media every other day; upon confluency, cells were harvested and stored in liquid nitrogen. When reconstituted, these primary non-transformed cells are grown in complete medium consisting of IMEM, heat inactivated 10% FBS, gentamicin and subsist for seven to eight passages. In this study all cells were used at passage 4. These outflow pathway cultures comprise all cell types involved in maintaining resistance to flow. That includes cells from the three distinct regions of the trabecular meshwork plus cells lining the Schlemm's canal. Because most of the cells in these cultures come from the trabecular meshwork, they are commonly referred to as "trabecular meshwork cells".

Delivery of Recombinant Adenoviruses to Primary Human Trabecular Meshwork Cells

Human trabecular meshwork primary cells at passage 4, seeded on either 3 cm or 10 cm dishes, were grown to between 65–90% confluency, washed twice with PBS and exposed to the recombinant adenoviruses (Adh.Q368X, Adh.R342K, Adh.D380N, Adh.K423E, Adh.MYOCWT and Ad5.CMV-Null) in 1 ml or 3 ml serum-free medium respectively. Multiplicity of infections (moi) ranged from 1.6×10^3 – 1.6×10^4 vg/cell and were randomly distributed among the replicas. After exposure to the virus for 90 min, complete media was added and incubation continued for 48 h or 72 h. Mutant-Null infections were always performed in the same day, but interspersed replicas expand over two years. Although FBS lot number was not recorded in each experiment, the same supplier, same catalog number of heat inactivated FBS was used in all experiments.

RNA Extraction, Reverse Transcription and TaqMan-PCR Assays

Human trabecular meshwork cells were scraped from tissue culture dishes with guanidine thiocyanate buffer (RLT, Qiagen, Valencia, CA). Total RNA was extracted by loading the solution onto a QIA ShredderTM column (Qiagen) and continued by the use of the RNeasy Mini kit with on-column RNase-free DNase digestion according to manufacturer's recommendations (Qiagen). Purified RNA was eluted in 30 µl RNase-free water and the concentration measured with a NanoDrop ND-100 spectrophotometer (Thermo Fisher Scientific). Total RNA recoveries averaged 65.4 ± 3.6 µg and 11.9 ± 1.1 µg per 10 and 3 cm culture dishes respectively. RNA quality was assessed by measuring the size distribution on an Agilent Bioanalyzer (Agilent Technologies, Santa Clara, CA).

Reverse transcription (RT) reactions were conducted with 1 µg HTM cells RNA in a 20 µl total volume of proprietary RT buffer with RNase inhibitor (High Capacity cDNA kit) (ABI) following manufacturer's recommendations (25°C 10 min, 37°C 2 h, 85°C 5 min, then 4°C). Fluorescently labeled TaqMan probe/primers sets for human MYOC, CSTA, CXCL2, IGF1, MMP1, MMP3, MMP12, SFRP1, STC1, SNCA, RAB39B, THBD and 18S RNA were purchased from the ABI TaqMan Gene Expression Assays (ABI). The human probes used were: *MYOC* (Hs00165345_m1), *CSTA* (Hs00193257_m1), *CXCL2* (Hs00235956_m1), *IGF1* (Hs00153126_m1), *MMP1* (Hs00233958_m1), *MMP3* (Hs00968305_m1), *MMP12* (Hs00899662_m1), *SFRP1*

(Hs00610060_m1), *STC1* (Hs00174970_m1), *SNCA* (Hs01103383_m1), *RAB39B* (Hs00293395_m1) and *THBD* (Hs000264920_s1). All but one probe corresponded to sequences from different exons. The 18S RNA probe corresponded to sequences surrounding position nucleotide 609 (Hs99999901_s1). Reactions were performed in triplicate 20 µl aliquots using TaqMan Universal PCR Master mix No AmpErase UNG, run on an Applied Biosystems 7500 Real-Time PCR System, and analyzed by 7500 System SDS v.2.0.4 software (ABI). Relative Quantification (RQ) values between treated and untreated samples were calculated by the formula $2^{-\Delta\Delta C_T}$ where C_T is the cycle at threshold, ΔC_T is C_T of the assayed gene minus C_T of the endogenous control (18S), and $\Delta\Delta C_T$ is the ΔC_T of the normalized assayed gene in the treated sample minus the ΔC_T of the same gene in the untreated one (calibrator). Because of the high abundance of the 18S rRNA used as the endogenous control and in order to get a linear amplification, RT reactions from treated and untreated samples were diluted 10^4 times prior to their hybridization to the 18S TaqMan probe. Statistical analysis was performed by the Student's *t*-test.

RNA Microarrays Hybridization

The RNAs from cells infected with *MYOC* mutants viral recombinants were prepared for hybridization to Human Genome U133 Plus 2.0 (n = 17) GeneChips (Affymetrix, Santa Clara, CA) at the University of North Carolina Functional Genomics Core Facility. These oligonucleotide microarrays contain 54,678 probe sets representing approximately 39,500 well-characterized human genes. The level of transcription of each gene represented on these chips is measured using the 11 nucleotide sequences which comprise each probe set. For the hybridization, total RNA (~0.7 µg) was reverse transcribed into cDNA using a cDNA kit from Life Technologies with a T7-(dT)₂₄ primer. Biotinylated cRNA was then generated from the cDNA reaction using the BioArray High Yield RNA Transcript Kit. The cRNA was then fragmented in fragmentation buffer (5X fragmentation buffer: 200 mM Tris-acetate, pH 8.1, 500 mM KOAc, 150 mM MgOAc) at 94°C for 35 min before the chip hybridization. 15 µg of fragmented cRNA was then added to a hybridization cocktail (0.05 µg/µl fragmented cRNA, 50 pM control oligonucleotide B2, *BioB*, *BioC*, *BioD*, and *cre* hybridization controls, 0.1 mg/ml herring sperm DNA, 0.5 mg/ml acetylated BSA, 100 mM MES, 1M [Na⁺], 20 mM EDTA, 0.01% Tween 20). 10 µg of cRNA was used for hybridization. Arrays were hybridized for 16 h at 45°C in the GeneChip Hybridization Oven 640. The arrays were washed and stained with R-phycoerythrin streptavidin in the GeneChip Fluidics Station 450. After this, arrays were scanned with the GeneChip Scanner 3000 7G Plus. Sample quality was assessed by examination of 3' to 5' intensity ratios of certain genes.

GeneSpring Analyses

Raw data CEL files from Affymetrix were imported into GeneSpring GX Expression Analysis software, version GS10 (Agilent Technologies). For analysis of expression changes between the *MYOC* mutants, *MYOC* wild-type and null infected samples, their files were pre-processed through the Robust Multichip Average (RMA) and replicas from each of the mutant, wild-type or control chips were grouped using the grouping feature of the program. An interpretation was created which identified the treated versus the control selecting average over replicates in each of the two conditions. To eliminate genes expressed at lower levels in at least one out of the conditions compared, normalized data

were filtered by expression level using the signal intensity raw data at a lower cutoff value of 50.

To identify top-changers, data were subsequently filtered on Fold Change (FC) to select genes that exhibited at least a 1.5-fold increase or decrease in the MYOC infected cells. Variance of the samples was obtained by the unpaired *t*-test. Lists with genes altered FC ≥ 1.5 were generated in GS10 and exported to the hard drive. These original gene lists contain many annotations with no Entrez number, repeated annotations with the same Entrez gene, a few annotations recognizing more than one Entrez number (almost identical genes, often pseudogenes) as well as genes encoding hypothetical proteins and undefined open reading frames genes. Using standard excel sorting applications, we used a rational approach to clean and filter FC 1.5-fold gene lists for each of the redundant and the undefined genes parameters (see results below). Heat maps of the full range FC of the mutants on categories of genes from a given function (calcification, elastin collagen crosslinking, WNT signaling pathway, stress and UPR response and molecular signature of glaucoma) were created in GS v7.3. The custom made gene-function lists contained one Affymetrix ID per gene. In the case that one of the genes from the list was represented by more than one Affymetrix ID in the chip, we chose the ID which was more altered by the Q368X mutation. Overlapping Venn diagrams were created in GS10 with re-imported gene lists containing Entrez numbers (IDs with no Entrez removed). Gene ontologies of the overlapping gene list altered in all-mutants were created in GS v7.3. They were obtained from the GO SLIMS lists available in the GS7 software, which contain subsets of the terms in the whole GO.

Microarray Data Submission

All microarray data is MIAME compliant and the raw data has been deposited in the ArrayExpress MIAME compliant database. The accession numbers of each of the five experiments along with login information are as follows:

Experiment name: MYOC.Q368XvsNull
ArrayExpress accession: **E-MEXP-3427**.
Username: Reviewer_E-MEXP-3427
Password: ebr8fswC

Experiment name: MYOC.R342KvsNull
ArrayExpress accession: **E-MEXP-3435**.
Username: Reviewer_E-MEXP-3435
Password: nzsut632

Experiment name: MYOC.D380NvsNull
ArrayExpress accession: **E-MEXP-3434**.
Username: Reviewer_E-MEXP-3434
Password: uuvvpXH4

Experiment name: MYOC.K423EvsNull
ArrayExpress accession: **E-MEXP-3439**.
Username: Reviewer_E-MEXP-3439
Password: Ljwhbanh

Experiment name: MYOC.WTvsNull
ArrayExpress accession: **E-MEXP-3440**.
Username: Reviewer_E-MEXP-3440
Password: kdXjkn3s

Plasmids and Transfections

A human *MYOC* full coding recombinant expression vector was generated by amplifying pMC2 with primers 5' CACCTGCAAT-GAGGTTCTTCTGTG3' (forward) and 5' TTTTCA-CATCTTGGAGAGCTTGAT3' using Platinum Taq DNA

Polymerase (Invitrogen) and cloning of the gel purified insert into pCDNA3.1D V5-His-TOPO (Invitrogen). The new plasmid, pKM1, contains 1522 bp (from -4ATG to TGA+3) of wild-type *MYOC* cDNA (19–1540 nt). A *MYOC*-V5 fused clone was generated by amplifying pKM1 with the same forward primer and a 5' TTTTCATCTTGGAGAGCTTGATGTC3' (reverse) which skips the stop codon (19–1534 nt) using high fidelity Advantage HD Polymerase Mix (Clontech). The gel purified fragment was incubated with pCDNA3.1D V5-His-TOPO to yield plasmid pMG29. A pCDNA3.1D V5-His-TOPO empty (CMV promoter, no transgene) was obtained during the sequence screening of above cloning procedures (pEmpty). All plasmids were transformed in TOP10 cells (Invitrogen) and confirmed by sequence. A TrueORFGold clone of human *CSTA* (stefin A) was obtained from Origene (Rockville, MD, cat.# RC203115). The pCSTA plasmid contains the full coding *CSTA* cDNA (nt 130–424 accession # NM_005213) fused to Myc-DDK tags. A TrueORF-Gold clone of human mutant *CSTA* (*CSTAm*) was designed and custom ordered to Origene. The *CSTAm* was obtained by site-directed mutagenesis of the codon GGA at nucleotide 10–12 of the ORF, coding for Glycine, to AGG coding for Arginine [37]. Change of the evolutionary conserved Gly-4 residue has been shown to decrease affinity of the binding of the *CSTA* inhibitor to Cathepsin B [37]. Plasmid DNAs were isolated either using either a Midi-Prep plasmid kit (QIAGEN) or a PowerPrep™ HP Plasmid Purification kit (Origene), which results in lower toxicity after the nucleofector transfection (unpublished).

Transfection of HEK293 cells was performed by the standard calcium phosphate method precipitating 7 μ g of DNA (pMG29:pCSTA or pEmpty 1:2.5) in 120 mM calcium phosphate (Clontech) per 3 cm dish, 40% confluent cells. After overnight exposure, cells were quickly washed with 1 mM EGTA/PBS, and incubated in IMEM 2% FBS for an additional 48 h. A change of medium was done 24 h before harvesting. Transfection of primary HTM cells was performed using nucleofector technology (Amaxa Lonza, Basel, Switzerland), their basic kit for Primary Mammalian Endothelial Cells and the protocol previously described [42]. Briefly, cells were split 24 h before transfection, trypsinized, counted, and centrifuged at 100 g for 10 min. Cell pellets were resuspended in the proprietary mammalian endothelial solution at a concentration of 4×10^5 cells/100 μ l. Plasmid DNA encoding the V5-fused *MYOC* protein (pMG29) was mixed with that of plasmids encoding either the DDK-fused *CSTA* (pCSTA) or an empty transgene (pEmpty) and added to the cells at a total of 3 μ g (pMG29:pCSTA or pEmpty 1:2). Cells-DNA solution was electroporated on the nucleofector apparatus (Amaxa Lonza) using program T-23 and allowed to recover for 15 min in pre-warmed serum-containing media inside the CO₂ incubator. Following the recovery period, cells were gently transferred to warm medium-containing 3 cm dishes. After 24 h, media was changed with IMEM 10% serum followed by replacement with serum-free media 8 h later. Cells were then maintained for an additional 24 h (48 h post transfection) before being harvested for the extraction of proteins.

Western-Blots and Antibodies

Proteins extracted from transfected HEK293 and HTM primary cells were assayed for levels of the different forms of the *MYOC* protein. Cultured media was collected and saved. Adhered cells were washed 2X with cold PBS and scraped from the dish with 100 μ l of modified RIPA buffer containing 1X protease inhibitor cocktail (Roche Applied Science, Indianapolis, IN). Aliquots of 4 μ l from either the cell lysates or the media were mixed (1:2 vol) with Laemmli buffer (Bio-Rad, Hercules, CA)

containing 5% β -mercaptoethanol and loaded onto 4–15% SDS-PAGE Tris-HCl polyacrylamide gels (Bio-Rad). After running, gels were electro-transferred to PVDF membranes (Bio-Rad), blocked with 5% nonfat dry milk (Bio-Rad) in PBS-0.2% Tween 20 (Sigma-Aldrich, Saint Louis, MO) for 2–5 h and incubated at 4°C for 3 h to overnight with anti-V5 mouse monoclonal antibody (Invitrogen) (1:400). Primary antibody reaction was followed by incubation with anti-mouse IgG secondary antibodies conjugated to horseradish peroxidase (1:2000; Pierce Biotechnology, Rockford, IL) for 1 h at room temperature. Immunoreactive bands were visualized by chemiluminescence ECL Plus western blotting detection system (GE Healthcare Biosciences, Piscataway, NJ) and membranes were exposed to X-ray film (BioMax MR; Kodak, Rochester, NY). For controls, blots were re-probed with a monoclonal anti β -actin (synthetic peptide) (Sigma) (1:5000) and a monoclonal anti-DDK (synthetic peptide) (1:200) (Origene) for 1 h at room temperature and overnight at 4°C, followed by anti-mouse IgG secondary antibodies conjugated to horseradish peroxidase (1:5000; Pierce Biotechnology). Full length and processed MYOC bands were captured using a Chemi System equipped with a GelCam 310 camera, PCI digitizing image acquisition board, EpiChem II Darkroom with transilluminator and VisonWorksLS image acquisition software v.7.0.1 (UVP, Upland, CA). Densitometry of each band was performed with the provided software to obtain mean intensity values (average of intensities of all pixels of band region, minus average intensity of the background pixels). Default background is equal to the sum total of the perimeter around each band region, three pixels wide. The percentage of the processed band in each treatment was calculated by dividing its mean density by the sum of the mean density of the process plus unprocessed bands.

Results

Adenoviral Vectors Carrying four MYOC Mutants Linked to Glaucoma

The adenoviral vectors were constructed as indicated in methods and the *MYOC* mutant proteins encoded by their inserted cassettes are shown in Figure 1. Prior to the generation of RNA to hybridize to the Affymetrix chips, the mutants vectors were tested on HTM cells for the overexpression of *MYOC* RNA and proteins using TaqMan PCR and WB as described above. Upon normalization to 18S, the levels of MYOC RNA on cells infected with each of the mutants over the levels of MYOC RNA on cells infected with Ad.Null increased significantly for all mutants. Infection with Adh.Q368X produced the truncated form of the protein while Adh.R342K, Adh.D380N and Adh.K423E produced the same size protein as the wild-type. Although the TaqMan mRNA levels produced by Adh.K423E mutant were similar to those of the other mutants, the levels of its produced protein were the lowest, indicating either a higher susceptibility to degradation of this MYOC mutant protein, or a lower recognition by the antibody due to faulty folding.

Number of Genes Altered in HTM Cells Overexpressing each of the Four MYOC Mutants

To gain a first insight into the extent of changes occurring in the transcriptome of HTM cells overexpressing *MYOC* mutants we counted the number of genes altered between the mutants and controls cells (cells infected with Ad5.CMV-Null viruses). To further understand the differences caused by the mutants and the wild-type, we re-analyzed the comparisons using the chips of the *MYOC* mutants versus those of the *MYOC* wild-type. To override the potential differences between primary cell lines derived from

different individuals, all overexpression experiments were conducted in the same cell line at the same passage (HTM-72, passage 4).

All comparisons were done using non-redundant lists of overexpressed genes. For this, the gene lists generated in Gene Spring were cleaned according to the following criteria. Affymetrix IDs that did not have an Entrez number were removed. In the few cases where one Affymetrix probe set ID number recognized more than one gene (usually almost identical genes or pseudogenes), one of them was selected. In the cases of redundant Entrez numbers, that is, when there were several Affymetrix IDs for the same Entrez number, we selected the ID that had been most altered.

Using replicas for each of the mutants and for the controls (Adh.MYOC $n = 10$, 2 per construct; Ad.CMV-Null $n = 7$) and selecting the methodology and filters outlined above, we generated lists of 1.5-fold altered genes. Out of the 54,678 spots in the array, the total number of non-redundant genes altered $\geq 1.5X$ was higher in the wild-type than in each of the mutants (Figure 2A). Overexpression of the wild-type induced the change of 4,337 genes while that of the Q368X mutation, which was the second highest, altered 2,603 genes. While the number of genes altered in the D380N (2,237) and K423E (2,283) mutations were pretty similar to those changed by the stop mutation, the mutation R342K induced only 803 changes in the HTM transcriptome (Figure 2A). From the total number of altered genes, the number of up- and downregulated seemed to be similar in wild-type and mutants with approximately one-half of the total altered in each category. The highest difference was observed in the R342K mutant, which had a higher number of downregulated genes (274 genes up- and 529 genes downregulated) (Figure 2A).

When comparing the number of genes altered in the mutants with those altered in the wild-type, we found that the stop mutation Q368X had the highest difference with a total of 6,716 (3,342 up and 3,374 down) (Figure 2B). Overall, looking at this parameter, it appeared that the mutants fell into two groups with considerably different patterns. The mutations Q368X and R342K had similar gene number changes and were much higher than those of D380N and K423E which in turn were similar to each other (1,411 and 1,384). Together this result on the absolute number of altered genes indicates that different *MYOC* mutants can alter the HTM transcriptome to a different extent and could therefore have a different severity outcome on the function of the tissue.

Selected Top-changers Trabecular Meshwork Relevant (TMR) Genes from MYOC Mutants Induced Lists

The 100 top-changers (50 upregulated and 50 downregulated) ($p \leq 0.05$) from each of the mutants compared to Ad5.CMV-Null are submitted as supporting material (Tables S1, S2, S3, and S4). To generate these lists we started with the non-redundant lists obtained above and rationally eliminated those ID numbers with annotations for LOC hypothetical proteins, FAM (family w/ sequence similarity), noncoding RNAs and pseudogenes. Myocilin was the most upregulated gene in all lists except in that of the K423E mutant, serving as a control of the overexpression. Levels of overexpressed *MYOC* were identical after infections with Q368X and R342K, and about half after D380N, though still at the top of the list (Tables S1, S2, S3, S4, S5, and S6). TaqMan PCR confirmed that the K423E mutant was highly overexpressing *MYOC*, so its absence from the top gene in the array list was interpreted as a low efficiency of this mutant's cDNA to hybridize to the *MYOC* Affymetrix gene chip spot.

To further get an insight into the extent of how many of those *MYOC* mutant-induced genes were encoding trabecular meshwork

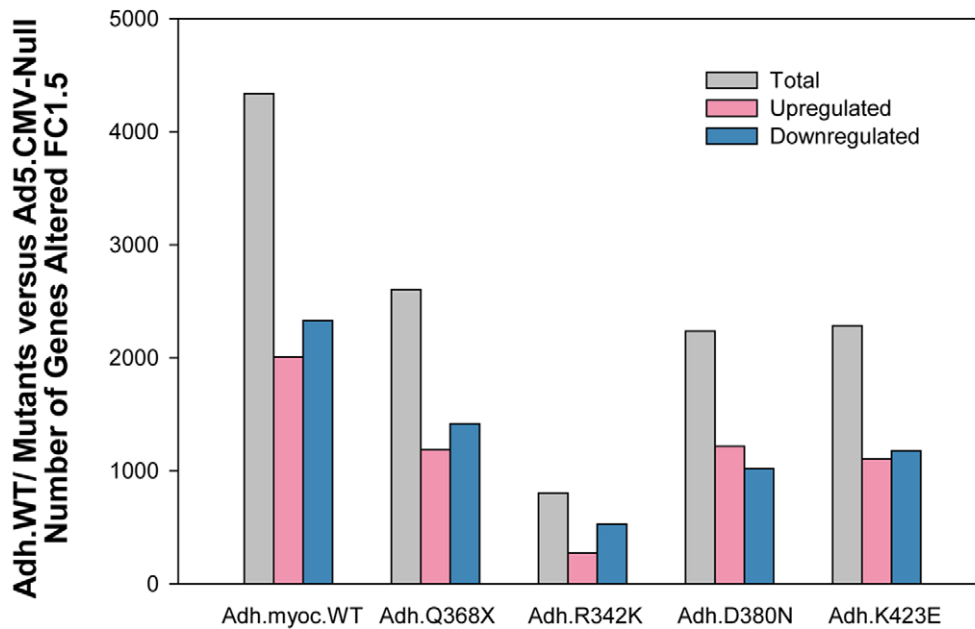
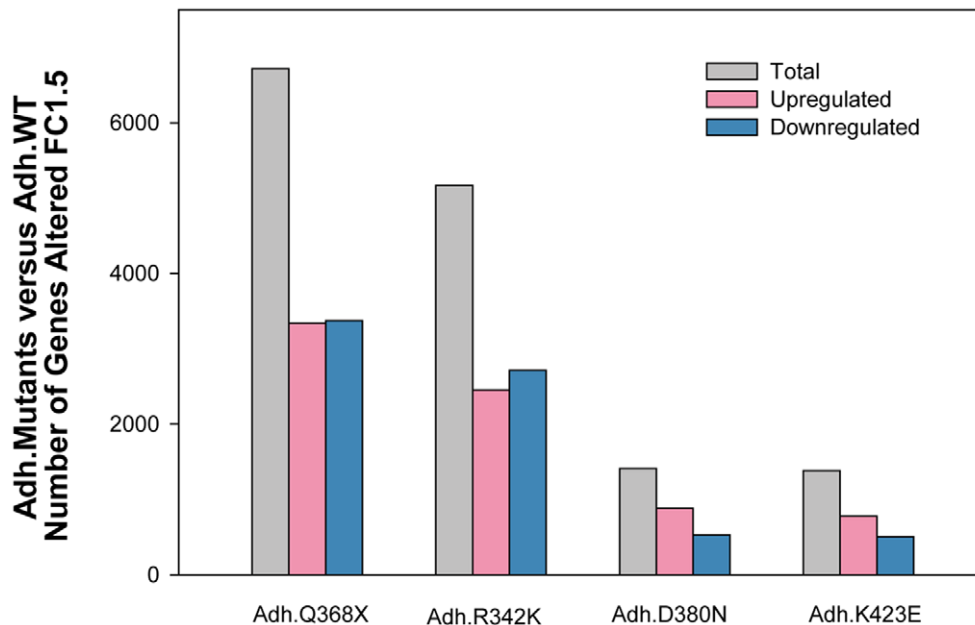
A.**B.**

Figure 2. Wild-type MYOC and different MYOC mutants alter different gene numbers on the trabecular meshwork transcriptome.

Adenoviral vectors carrying either wild type, four MYOC mutations cassettes or no transgene (Ad5.CMV-Null) were infected on primary human trabecular meshwork cell line HTM-72 to overexpress MYOC proteins. The expression of genes in the wild-type or mutant-treated cells was obtained using Affymetrix GeneChips (n = 17). GeneSpring 10 and Excel software were used to generate non-redundant gene lists with cutoff fold-change values of \geq and \leq 1.5. A: number of genes altered in cells treated with the wild-type or each of the mutants compared with the number altered in cells treated with the empty virus (Adh.WT/Mutants versus Ad5.CMV-Null). B: number of genes altered in cells treated with the each of the mutants compared with the number altered in cells treated with the wild type virus (Adh.Mutants versus Adh.WT).

doi:10.1371/journal.pone.0036301.g002

A. Rationally selected 20 TMR upregulated genes in the MYOC mutants

<i>Adh.Q368X vs Ad.Null</i>				<i>Adh.R342K vs Ad.Null</i>			
Gene Name	Symbol	FC	Entrez ID	Gene Name	Symbol	FC	Entrez ID
Tachykinin 1 (Substance P)	TAC1	43.2	6863	Tachykinin 1 (Substance P)	TAC1	13.4	6863
Lysosomal-associated membrane 3	LAMP3	28.5	27074	Spexin	C12orf39	6.1	80763
Spexin	C12orf39	12.0	80763	Lysosomal-associated membrane 3	LAMP3	4.6	27074
Ras-related protein 39B	RAB39B	10.2	116442	Heat shock 70KDa protein 5	HSPA5	3.3	3309
Cadherin 15 (M-cadherin)	CDH15	9.7	1013	Ras-related protein 39B	RAB39B	3.2	116442
Heat shock 70KDa protein 5	HSPA5	5.9	3309	Cystatin A (stefin A)	CSTA	3.2	1475
Protein disulfide isomerase A4	PDIA4	4.6	9601	Cadherin 15 (M-cadherin)	CDH15	2.7	1013
Interleukin 1 receptor-like 1	IL1RL1	4.1	9173	Osteoglycin	OGN	2.2	4969
Cystatin A (Stefin A)	CSTA	3.4	1475	Protein disulfide isomerase A4	PDIA4	2.1	9601
Stanniocalcin 2	STC2	2.4	8614	Extracellular matrix protein 2	ECM2	2.1	1842
Apoptosis regulator Bcl2	BCL2	2.3	596	Lysyl oxidase	LOX	1.9	4015
Calreticulin	CALR	2.3	811	Apoptosis regulator Bcl2	BCL2	1.8	596
Talin 2	TLN2	2.2	83660	Osteomodulin	OMD	1.8	4958
Nerve growth factor	NGF	2.1	4803	Prostacyclin I2 synthase	PTGIS	1.7	5740
Extracellular matrix protein 2	ECM2	2.1	1842	Nerve growth factor	NGF	1.7	4803
Calnexin	CANX	1.9	821	Intercellular adhesion molecule 1	ICAM1	1.7	3383
Matrix metalloproteinase 1	MMP1	1.9	4312	Interleukin 1 receptor-like 1	IL1RL1	1.6	9173
Dentin sialoprotein	DSPP	1.6	1834	Calnexin	CANX	1.6	821
Fibrillin 2	FBN2	1.6	2201	Caldesmon 1	CALD1	1.6	800
Neuregulin 1	NRG1	1.5	3084	Stanniocalcin 2	STC2	1.5	8614

<i>Adh.D380N vs Ad.Null</i>				<i>Adh.K423E vs Ad.Null</i>			
Gene Name	Symbol	FC	Entrez ID	Gene Name	Symbol	FC	Entrez ID
Aldo-keto reductase 1	AKR1C1	3.8	1645	Insulin-like growth factor 1	IGF1	3.9	3479
Angiopoietin-like 2	ANGPTL2	3.7	23452	Podoplanin	PDPN	3.8	10630
Aldehyde dehydrogenase 5 A1	ALDH5A1	3.5	7915	Selenoprotein P1	SEPP1	3.0	6414
Chemokine (C-X-C motif) ligand 12	CXCL12	3.3	6387	Angiopoietin-like 2	ANGPTL2	2.9	23452
Growth arrest-specific 1	GAS1	2.5	2619	Chemokine (C-X-C motif) ligand 12	CXCL12	2.5	6387
Synuclein alpha	SNCA	2.5	6622	Fibronectin 1	FN1	2.4	2335
Eukaryotic elongation factor 1 A1	EEF1A1	2.3	1915	Ras-related protein 39B	RAB39B	2.3	116442
Podoplanin	PDPN	2.3	10630	Matrix Gla protein	MGP	2.1	4256
Cathepsin O	CTSO	2.2	1519	Synuclein alpha	SNCA	2.1	6622
Prostacyclin I2 synthase	PTGIS	2.1	5740	Prostaglandin F receptor	PTGFR	2.0	5737
Ras-related protein 39B	RAB39B	2.1	116442	Caldesmon 1	CALD1	2.0	800
Extracellular matrix protein 2	ECM2	1.9	1842	Aldo-keto reductase 1	AKR1C1	2.0	1645
Lysosomal-associated membrane 2	LAMP2	1.9	3920	Cystatin A (stefin A)	CSTA	1.8	1475
Fibronectin 1	FN1	1.8	2335	Cathepsin O	CTSO	1.7	1519
Osteoglycin	OGN	1.7	4969	Bone morphogenetic protein 2	BMP2	1.7	650
Pigment epithelium-derived factor	PEDF	1.7	5176	Stanniocalcin 2	STC2	1.7	8614
Angiopoietin-like 7	ANGPTL7	1.7	10218	Fibrillin 1	FBN1	1.7	2200
Cathepsin F	CTSF	1.7	8722	Extracellular matrix protein 2	ECM2	1.6	1842
Insulin-like growth factor 1	IGF1	1.5	3479	Lysosomal-associated membrane 3	LAMP3	1.6	27074
Cystatin A (stefin A)	CSTA	1.5	1475	Eukaryotic elongation factor 1 A1	EEF1A1	1.5	1915

B.**Rationally selected 20 TMR downregulated genes in the MYOC mutants**

<i>Adh.Q368X vs Ad.Null</i>				<i>Adh.R342K vs Ad.Null</i>			
Gene Name	Symbol	FC	Entrez ID	Gene Name	Symbol	FC	Entrez ID
Stanniocalcin 1	STC1	-5.4	6781	Matrix metalloproteinase 1	MMP1	-4.5	4312
Sphingosine-1-phosphate receptor 3	S1PR3	-4.1	1903	Microtubule-assoc protein 2	MAP2	-2.8	4133
Insulin-like growth factor binding protein 5	IGFBP5	-3.6	3488	Parathyroid hormone-like hormone	PTHLH	-2.4	5744
Chemokine (C-X-C motif) ligand 12	CXCL12	-3.0	6387	Sphingosine-1-phosphate receptor 3	S1PR3	-2.4	1903
Microtubule-assoc protein 2	MAP2	-2.8	4133	Matrix metalloproteinase 12	MMP12	-2.1	4321
Parathyroid hormone-like hormone	PTHLH	-2.8	5744	Secreted frizzled-related protein 1	SFRP1	-1.9	6422
Secreted frizzled-related protein 1	SFRP1	-2.5	6422	Chemokine (C-X-C motif) ligand 12	CXCL12	-1.9	6387
Cytochrome P450, 26B	CYP26B1	-2.5	56603	Cytochrome P450, 26B	CYP26B1	-1.8	56603
Thrombospondin 2	THBS2	-2.5	7058	Stanniocalcin 1	STC1	-1.8	6781
Thrombomodulin	THBD	-2.2	7056	Thrombomodulin	THBD	-1.8	7056
Podoplanin	PDPN	-2.1	10630	Periostin, osteoblast specific factor	POSTN	-1.7	10631
Insulin-like growth factor 1	IGF1	-2.1	3479	Angiopoietin 2	ANGPT2	-1.7	285
Synuclein alpha	SNCA	-2.1	6622	Dickkopf homolog 1	DKK1	-1.7	22943
Lysyl oxidase-like 1	LOXL1	-2.0	4016	Procollagen C-endopeptidase enhancer 2	PCOLCE2	-1.7	26577
Matrix Gla protein	MGP	-2.0	4256	Insulin-like growth factor 1	IGF1	-1.6	3479
Osteoglycin	OGN	-1.9	4969	Follistatin	FST	-1.6	10468
Endothelin 1	EDN1	-1.9	1906	Endothelin 1	EDN1	-1.6	1906
Interleukin 8	IL8	-1.8	3576	Carbonic anhydrase II	CA2	-1.5	760
Angiopoietin 2	ANGPT2	-1.8	285	Tenascin C	TNC	-1.5	3371
Biglycan	BGN	-1.8	633	Stathmin	STATH	-1.5	6779

<i>Adh.D380N vs Ad.Null</i>				<i>Adh.K423E vs Ad.Null</i>			
Gene Name	Symbol	FC	Entrez ID	Gene Name	Symbol	FC	Entrez ID
Matrix metalloproteinase 1	MMP1	-5.5	4312	Matrix metalloproteinase 12	MMP12	-4.0	4321
Matrix metalloproteinase 12	MMP12	-5.3	4321	Lysyl oxidase-like 2	LOXL2	-3.0	4017
Tenascin C	TNC	-3.9	3371	Matrix metalloproteinase 3	MMP3	-2.8	4314
Versican	VCAN	-3.7	1462	Lysyl oxidase	LOX	-2.8	4015
Parathyroid hormone-like hormone	PTHLH	-3.3	5744	Cytochrome P450, 1B1	CYP1B1	-2.7	1545
Dickkopf homolog 1	DKK1	-3.2	22943	Calmodulin 1	CALM1	-2.7	801
Claudin 1	CLDN1	-3.1	9076	Heat shock protein 90	HSP90AB	-2.5	3326
Matrix metalloproteinase 3	MMP3	-3.0	4314	Claudin 1	CLDN1	-2.4	9076
Stanniocalcin 1	STC1	-2.5	6781	Interleukin 8	IL8	-2.2	3576
Endothelin 1	EDN1	-2.5	1906	Zyxin	ZYX	-2.0	7791
Interleukin 8	IL8	-2.3	3576	Presenilin 1	PSEN1	-2.0	5663
Angiopoietin 2	ANGPT2	-2.0	285	Biglycan	BGN	-1.9	633
Thrombomodulin	THBD	-2.0	7056	Endothelin 1	EDN1	-1.8	1906
Periostin, osteoblast specific factor	POSTN	-1.9	10631	Calreticulin	CALR	-1.8	811
Carbonic anhydrase II	CA2	-1.9	760	Calnexin	CANX	-1.8	821
Microtubule-assoc protein 2	MAP2	-1.8	4133	Stanniocalcin 1	STC1	-1.7	6781
Interleukin 6	IL6	-1.8	3569	Insulin-like growth factor binding protein 5	IGFBP5	-1.7	3488
Neuregulin 1	NRG1	-1.6	3084	Neuregulin 1	NRG1	-1.6	3084
Osteomodulin	OMD	-1.6	4958	Angiopoietin 2	ANGPT2	-1.5	285
Secretogranin II	SCG2	-1.6	7857	Secreted frizzled-related protein 1	SFRP1	-1.5	6422

Figure 3. *MYOC* mutants' top-changers contained numerous human trabecular meshwork relevant genes. Adenoviral vectors carrying four *MYOC* mutations cassettes and no transgene (Ad5.CMV-Null) were infected on primary human trabecular meshwork cell line HTM-72 to overexpress *MYOC* mutant proteins. The expression of genes in the mutant-treated cells was compared with that of the cells treated with the empty virus, using Affymetrix GeneChips (n = 15). Non-redundant gene lists from the cutoff FC value of \geq and \leq 1.5 of each mutant were screened for trabecular meshwork relevant (TMR) genes. Each selected TMR gene was manually cross-checked to identify its expression in the other three mutants. A: twenty selected upregulated TMR genes in Q368X, R342K, D380N and K423E. B: twenty selected downregulated genes in Q368X, R342K, D380N and K423E.
doi:10.1371/journal.pone.0036301.g003

functions, and to investigate whether there was sharing of genes among the four mutants, we screened each of the FC 1.5 lists for TMR. For this analysis, we separated the up- and downregulated genes of each mutant list, sort them by FC and, without taking into account the microarray p-values, scrolled down to rationally select 20 genes from each direction with TM and/or glaucoma-related functions (TMR) (total 160 genes). Then, we performed a manual cross-check and identified whether each of the selected genes in each mutant was present in the other three (Figure 3A and 3B).

Overall, we had a total of 75 unique TMR genes altered in any of four *MYOC* mutants, many of which had previously been reported as responders to glaucomatous insults in independent studies. Eight genes were altered in all the mutants. *Ras-related protein 39B* (*RAB39B*), *Cystatin A* (*CSTA*) and *Extracellular matrix protein 2* (*ECM2*) were upregulated, while *Endothelin 1* (*EDN1*), *Angiopoietin 2* (*ANGPT2*) and *Stanniocalcin 1* (*STC1*) were downregulated. *Chemokine (C-X-C) ligand 12* (*CXCL12*) and *Insulin-like growth factor 1* (*IGF1*, *Somatomedin C*) showed different regulation depending on the mutants.

The upregulated TMR genes induced by the Q368X mutant appeared to be more similar to those induced by R342K and different from those induced by D380N and K423E. Thus, including the all-common genes, 14 out of the 20 TMRs (70%) in Q368X were shared by R342K while only 6 and 7 in each of these were shared by either D380N and/or K423E respectively. Interestingly, upregulated D380N and K423E lists shared a higher similarity between themselves (12 out of 20, 60%).

The downregulated TMR genes induced by the Q368X, were however very similar in the four mutants. Thirteen out of 20 downregulated TMR in Q368X were altered in R342K and all genes but one, *Lysyl oxidase-like 1* (*LOXLI*), were altered in D380N and K423E. *LOXLI*, a gene recently linked to pseudoexfoliation glaucoma [43] was altered only by the Q368X mutation.

Among the altered genes shared by Q368X and R342K (mutant set #1) and not by D380N and K423E (mutant set #2), were *Tachykinin 1* (*TAC1*), *Protein disulfide isomerase A4* (*PDIA4*), *Cadherin 15* (*CDH15*), *Apoptosis regulator BCL2* (*BCL2*) and *CYP26B1*. The *TAC1* gene, encoding the precursor of neuropeptide substance P, was previously identified as a mechanosensitive gene in the human trabecular meshwork intact tissue [22,44]. Protein disulfide isomerase A4, which plays a key role in protein folding, had been found to be altered by TGF β 2, DEX and by elevated IOP in the trabecular meshwork tissue during the homeostatic response period [44–46].

Among the genes altered by set #2 and not by set #1 mutants we found Aldo-ketoreductase 1 (*AKR1C1*), Angiopoietin-like 2 (*ANGPTL2*), Fibronectin 1 (*FN1*), Matrix metalloproteinase 3 (*MMP3*) and α -Synuclein (*SNCA*), which affect various functions, such steroid metabolism, inflammatory signaling and ECM organization. The synucleins are proteins highly expressed in the brain and are involved in presynaptic signaling and membrane trafficking.

Two of the all-common genes (*IGF1* and *CXCL12*) support the notion that mutant's set #1 had similar effects on the trabecular

meshwork transcriptome, which were different from those of set #2. Expression of *IGF1* and *CXCL12* was down in set #1 and up in set #2. Insulin growth factor 1 was classified as an individual responder to elevated IOP in human perfused organ cultures and pressure [22] while *CXCL12* is a member of the same chemokine family as *CXCL2*, a general responder to elevated IOP. Another case where *MYOC* mutants had opposite effects on a given gene was that of *Podoplanin* (*PDPN*), a lymphatic marker regulated by elevated IOP. Podoplanin is upregulated by D380N and K423E while is downregulated by Q368X.

There were only a few TMR genes that were altered by just one mutant. These were: *Lysyl oxidase-like 1* (*LOXLI*) (downregulated by Q368X), *Procollagen C-endopeptidase enhancer 2* (*PCOLCE2*) (downregulated by R342K), *Pigment epithelium-derived factor* (*PEDF*) (downregulated by D380N), *Lysyl oxidase-like 2* (*LOXL2*) and *Cytochrome P450 1B1* (*CYP1B1*) (downregulated by K423E), and *Bone morphogenetic protein 2* (*BMP2*) and *Fibrillin 1* (*FBN1*) (upregulated by K423E). Curiously, three of these genes have been genetically linked to glaucoma [43,47,48], suggesting an additional physiological link of the mutants with glaucoma at the molecular level.

Another trabecular meshwork gene previously known to be altered under other insults (IOP and DEX) was *Thrombomodulin* (*THBD*) [45]. Thrombomodulin is a vascular endothelial cell receptor that binds to thrombin and is involved in the inhibition of blood clotting. It has been speculated that *THBD* plays a role in maintaining the fluidity of the aqueous humor [45]. In this study, *THBD* was downregulated in all but the K423 mutant, suggesting a potential detrimental effect caused by the *MYOC* mutants. The same occurred with insult-altered metalloproteinases *Matrix metalloproteinase 3* (*MMP3*) (*Stromelysin 1*) [49] and *Matrix metalloproteinase 12* (*MMP12*) (*Macrophage elastase*) [22] which were shown downregulated here by the *MYOC* mutants suggesting that they would contribute to a decrease outflow.

Although many of the rationally selected TMR genes had significant microarray FC values, some of them had not. Thus, a representative sample of ten genes with no significant microarray p-values in at least one mutant were analyzed in triplicate by the more rigorous TaqMan PCR assay in a different primary cell line. HTM-137 and HTM-134 lines were infected with Adh.Q368X, Adh.R342K, Adh.D380N, Adh.K423E plus the control Ad.Null viruses, their RNA extracted at 48 h post-infection and reversed transcribed. Results are included in Table S5. Although not in every case the absolute TaqMan FC alteration value was similar to that of the microarray data (different individual, different culture and different viral stock), only four of the forty TaqMan assays performed showed a p-value higher than 0.05. Of the four (*MMP1* and *SFRP1* in Adh.Q368X and *MMP12* and *SFRP1* in Adh.K423E), two of them had a p<0.05 in the microarrays (Table S5). The remaining of the genes exhibited highly significant p-values in all mutants (Table S5).

Altogether these results indicate that overexpression of *MYOC* mutants share many elicited changes with other known glaucomatous insults. Further, they indicate that distinct *MYOC* mutants

could have specific effects on the trabecular meshwork cells transcriptome.

Pattern of Expression of Trabecular Meshwork Relevant Functions (TMR.F) Gene Lists in the Four MYOC Mutants

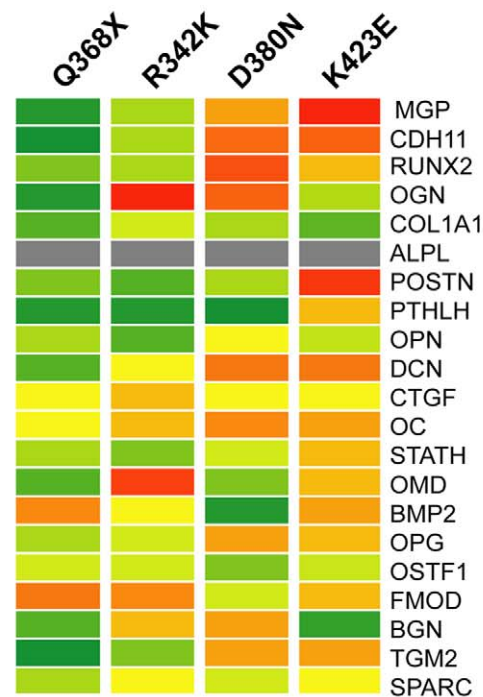
Next we investigated the overall expression pattern of set of genes known to be associated with selected TMR.F. In other words, we wanted to know whether genes involved in calcification mechanisms [50], collagen-elastin cross-linking functions [51], the WNT signaling pathway [22,25,26] and stress response had been affected by overexpression of *MYOC* mutants. We custom made comprehensive gene lists of the four mechanisms each containing 20–21 genes, and ran heat maps against the complete FC lists of each of the *MYOC* mutants (Figure 4). Each row of the map represents the response of a single gene to the overexpression of each of the four *MYOC* mutants, expressed in FC of the *MYOC* mutant- versus Ad5.CMV-Null infected cells. Each column represents the set of genes selected per category. The range of the FCs of the genes in the calcification, collagen-elastin and WNT maps by all mutants was between +2.1- and –3.3-fold. The range of FC of the stress and UPR genes was much larger, between +8.5 and –2.0-fold. Altered *MYOC* mutant genes which did not pass the minimal expression criteria (absent signals) have no color and appear as gray-cells. Overall, most of the genes of in each of the four functional categories were up or down regulated by at least one of the *MYOC* mutants and only a few were not affected in any mutant (represented by yellow colors). The trend of the similarities of the mutants in set #1 distinct from those in set #2 can be also seen here, mostly on genes with highest or lowest changes.

Calcification genes. The mutation Q368X downregulated most of the genes in the calcification category, including *Matrix Gla (MGP)*, an inhibitor of calcification and one of the ten most abundant genes in the trabecular meshwork [52,53]. Concurrently, Q368X upregulated *BMP2*, an inducer of calcification and bone formation which loses its activity upon binding to the inhibitor *MGP* [54]. These two changes together would suggest that the Q368X mutant is prone to induce calcification in the HTM cells which in turn would provoke hardening of the tissue and reduce outflow facility. In contrast, the same *MGP* gene was upregulated in the set #2 mutants, where *BMP2* was moderately reduced, indicating a different degree of involvement of this pathway by different *MYOC* mutants. The *Connective Tissue Growth Factor (CTGF)* gene, which has been extensively studied for its relevance in ECM deposition in trabecular meshwork function [55] was the less altered in all mutants, and *Collagen type 1 alpha 1 (COL1A1)*, an important structural component of the trabecular meshwork ECM, was downregulated in the four mutants assayed. Genes like *Osteomodulin (OMD)* and *Osteoglycin (OGN)*, also known as *Mimcan*, members of the SLPRs family of proteoglycans were markedly upregulated only by mutant R342K and appeared downregulated by Q368X. These two genes are markers of osteoblast differentiation [56], and respond to mechanical stress [44,46]; *OGN* was found upregulated in tissues from POAG patients [57]. Another gene, *Periostin (POSTN)*, also known as *Osteoblast-specific factor 2*, secreted by osteoblasts, was highly upregulated only in K423E. Periostin was previously shown to be upregulated by the glaucomatous insults of mechanical strain and TGFβ2 [58,59]. Lastly, *Transglutaminase 2 (TGM2)*, which catalyzes the cross-linking of numerous ECM proteins, whose presence in vascular smooth muscle cells (VSMC) is key to mineralize their matrix and which is present in the aqueous humor of glaucomatous patients [60] was very much downregulated in Q368X (Figure 4 upper left panel).

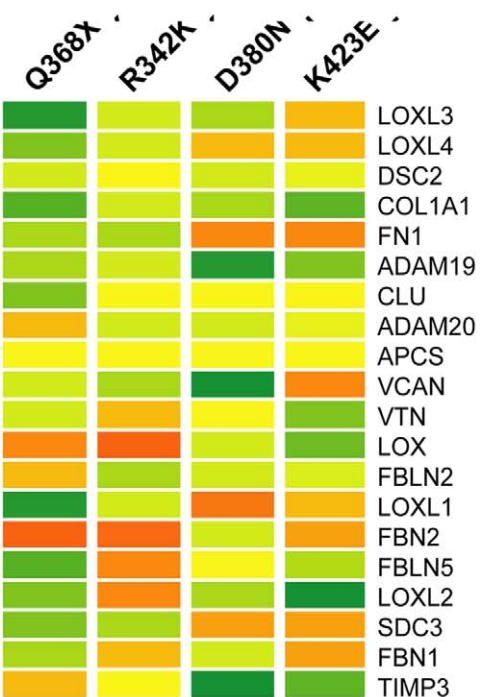
Collagen-Elastin Crosslinking. The most upregulated genes in this TMR.F category were *Fibrillin 2 (FBN2)* and to a lesser extent *Lysyl oxidase (LOX)*. They were induced with different intensities in mutant's set #1 Q368X and R342K. Lysyl oxidase is an enzyme involved in post-translational modifications of collagen and elastin and in the formation of intra/intermolecular cross-links, and *FBN2* is involved elastic fiber assembly. Lysyl oxidase-like 1, which is linked to Pseudoexfoliation (PEX) glaucoma, and which is heavily bound to the PEX material of PEX patients was very downregulated in Q368X, while other two PEX relevant components [51], *FBN1* and *Fibulin 5 (FBLN5)*, were slightly altered in all four mutants. The mutation D380N most downregulated *Versican (VCAN)*, another PEX component and mechanical strain regulated gene [44], and two metalloproteinases/inhibitors, *ADAM metalloproteinase 20 (ADAM20)* and *Tissue inhibitor of metalloproteinases 3 (TIMP3)*, which are involved in maintaining the balance of the ECM and therefore affecting the elastin network. Overall it seemed that the effect of the four *MYOC* mutants had subtle effects on genes involved in the formation of the elastin network and that such light effect was mostly that of downregulation (Figure 4 right panel).

WNT signaling. Genes involved in this pathway were downregulated preferentially by mutant's set #1. Mutant Q368X most downregulated *Secreted frizzled-related protein 1 (SFPR-1)*, an IOP responder gene [22] which is present in glaucomatous trabecular meshwork cells and causes elevated pressure [26]. The most differently regulated gene between set #1 and set #2 was *Transcription factor 4 (TCF4)*, which interacts with β-catenin and mediates transcription of WNT targeted genes. The upregulation of *TCF4* in D380N and K423E could be an indication that these two *MYOC* mutants would utilize more the WNT pathway to induce transcription than the other two. In contrast, *Dickkopf-1 (DKK-1)*, an antagonist that prevents activation the WNT pathway, was downregulated by all mutants, especially by D380N. Two of the genes of this pathway, the intronless transmembrane receptor *Frizzled family receptor 10 (FZD10)*, and the WNT protein inhibitor *WNT inhibitory factor 1 (WIF1)*, were not expressed in these set of trabecular meshwork cells (Figure 4, lower left panel).

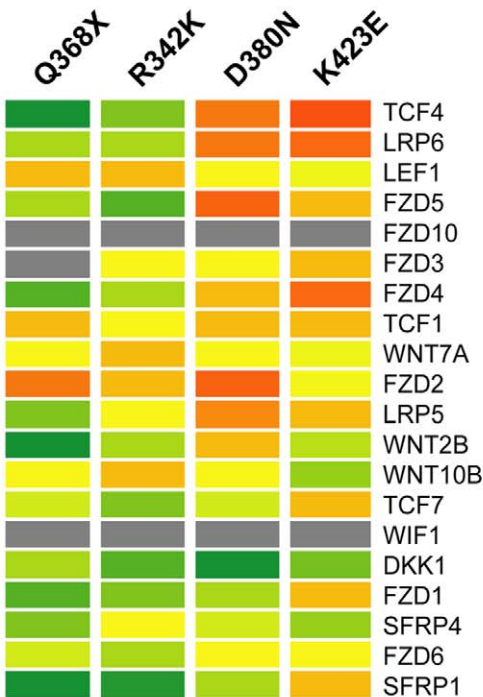
Stress and Unfolded Protein Response (UPR). Because *MYOC* mutants are known to accumulate in the ER and thus affect the UPR [11,18,19,23], we next examined the expression of twenty genes encoding the most common stress proteins (Figure 4, lower right panel). We found that expression of genes in the stress category was considerably affected by the *MYOC* mutants. Furthermore, expression of these genes was clearly different in set #1 and #2 mutants. The mutant having a major effect on this TMR.F was the stop mutation Q368X. In this mutant, the expression of all but two of the selected most commonly associated proteins were markedly altered. Among them the canonical UPR proteins *Bone-inducing protein (BIP)*, *DAN-damage-inducible transcript 3 (CHOP)* and *Calreticulin (CALR)* were markedly upregulated, as well as chaperones *Der1-like protein 3 (DERL3)* and heat shock proteins *HSP90B1*, *DNAJB9* and *DJC6*. Interestingly, *CALR*, an ER Ca²⁺ binding protein that binds to the glucocorticoid receptor, together with *Stress-induced-phosphoprotein 1 (STIP1)* was one of the most down regulated protein in the set #2 mutants. Another protein in which the direction of expression was clearly reversed in both sets was *SNCA*, an important component of the amyloid plaques in Alzheimer patients. *SNCA* was the most UPR upregulated transcript in D380N and K423E and the most downregulated in Q368X and R342K. Except for the *NADH dehydrogenase (ubiquinone) 1 alpha subcomplex, assembly factor 1 (NDUFAF1)*, the UPR proteins altered in transgenic flies carrying these mutants [19] are also



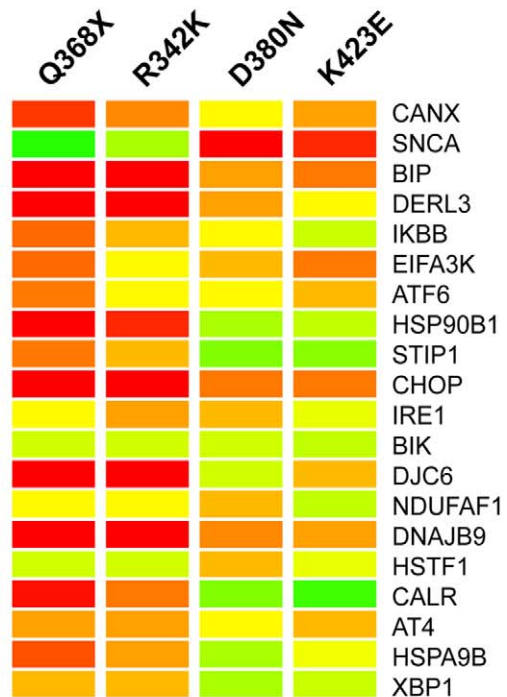
Calcification genes



Collagen-Elastin crosslinking genes



WNT signaling pathway genes



Stress and Unfolded Protein Response genes

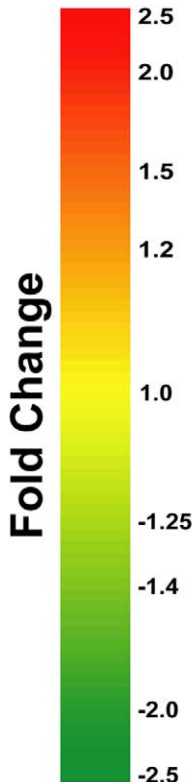


Figure 4. *MYOC* mutants induced changes on genes of trabecular meshwork relevant functions, especially on the UPR. Heat maps of set of genes representing four relevant trabecular meshwork functions. The four categories gene lists were costumed generated by literature review. Each row represents the fold change (Adeno.*MYOC* mutant over Adeno.Null) for a single gene in each of the four mutants. Each column represents the fold changes for all genes of the category in one *MYOC* mutant. The fold change for each gene is visually represented by a color, which is given by the scale bar in the center of the figure. Heat maps were generated with genes lists containing the full range of fold changes. Gray cells indicate that the expression of the giving gene was below the signal intensity cutoff value and was considered absent.
doi:10.1371/journal.pone.0036301.g004

altered in the human trabecular meshwork tissue, validating the fly system as a good genetic model of glaucoma.

Pattern of Expression of the Physiological Trabecular Meshwork Biomarkers Gene List in the Overexpressed Four *MYOC* Mutants

We next were interested to determine the ability of the *MYOC* mutants to alter a set of genes potentially associated with glaucoma and or glaucomatous insult. The 50 gene list is based on a previously published potential molecular signature of glaucoma genes [45]. It is also based on a more recent list of physiological biomarkers of glaucoma built on a revision of trabecular meshwork gene expression studies from us and other investigators (Table S6). The results of the heat map showing the expression of the 50 genes in all the mutants are shown in Figure 5. All genes except *Endothelial adhesion molecule 1 (ELAMI)* were present in all the mutants, indicating that *ELAMI* did not pass the filter set up for analysis of expression in the HTM-72 cell line. Because expression of this gene has been detected in whole trabecular meshwork tissues [22], its absence here indicates a marked downregulation of the gene when the cells are set up in culture.

Although some of the genes were expressed in set #1 differently than in set #2, the overall patterns of the different sets was not as marked as seen in the other gene lists categories. It is interesting to observe that 78% of the genes from this independent gene list were shown to be altered more $\geq 1.5X$ in at least one of the four *MYOC* mutants (Tables S1, S2, S3, S4, and Figure 3A and Figure 3B), an indication of the physiological causative role of *MYOC* in glaucoma. Very few genes were altered in the same direction in all four mutants. Two of the three downregulated genes, *EDN1* and *MMP12*, had been mentioned above. The third one, *Parathyroid hormone-like hormone (PTH1H)*, is a protein that regulates vascular calcification [61] and that has previously been shown to be induced by DEX in the trabecular meshwork [62]. Only the gene encoding *Prostaglandin D2 synthase (PTGDS)*, an enzyme that catalyzes the conversion of PGH2 to PGD2, was lightly upregulated in the four mutants.

Overall, a similar number of genes were up- and downregulated in mutants Q368X, D380N and K423E while R342K showed a lower number of downregulated genes. However, alteration of specific genes varied. The genes most altered by Q368X were *TAC1*, *CDH15*, *PDIA4* and *HSP90B1* (upregulated 43X, 9.7X, 4.6X and 3.3X respectively), and *PTH1H*, *SFRP1* and *Thrombospondin2 (THBS2)* (all downregulated $-2.5X$). The mutant R342K shared the four most upregulated and two of the most downregulated (*PTH1H*, *SFRP1*) with Q368X. Interestingly, the gene most downregulated by R342K, *MMP1* ($-4.5X$), was shared with the D380N and K423E mutants but not with Q368X, where *MMP1* was upregulated. Mutants D380N and K423E shared *PDPN* among their three top upregulated and the metalloproteinases *MMP3* and *MMP12* among the top downregulated. Another interesting difference among the effect of the four mutants on the transcriptome was the total lack of expression of *TAC1* (precursor of the substance P neuropeptide) in D380N and K423E, while it was the most induced gene in Q368X and R342K. Mutant Q368X was the only one to exhibit genes with unique responses,

that is, with changes in expression that were opposite to the changes incurred by the other three (*MMP1*, *MMP3* and *Prostacyclin synthase, PTGIS*).

Of the four genes induced by the highest number of glaucomatous insults, *Angiopoietin-like 7 (ANGPTL7)*, *PDIA4*, *Superoxide dismutase 1 (SOD1)* and *Tropomyosin 4 (TPM4)* (Table S6), only *PDIA4* (upregulated in Q368X and R342K), and *TPM4* (downregulated in K423E) were markedly altered in some of the mutants. *PDIA4* is an ER protein with isomerase activity on S-S bonds, and *TPM4* is actin binding protein involved in the contractile system of the cell.

Altogether, these different and common influences on the transcriptome triggered by the four mutants reveal a potential molecular reason as to why each of the *MYOC* mutants have a distinct clinical outcome and affect a particular group of the population.

Genes Altered in All Mutants

In addition to finding genes by which each of the mutants may exert their damage, we were interested in searching for a common altered gene whose mechanism of action could potentially be applied to all *MYOC*-causing glaucomas. For this we compared the 1.5X altered genes from wild-type (Adh.*MYOCWT*) and Adh.Mutants using the Venn map feature of the GS10 program. Because this feature uses the Affymetrix ID numbers for the comparisons, for this analysis we used 1.5-fold redundant gene lists (all spots for a given Entrez number included). Fold change ≥ 1.5 lists of each of the wild-type and mutants versus the null virus were created as indicated in methods, exported to the hard drive, and cleaned of IDs that did not have an Entrez number.

To first get an insight on the extent of sharing changes between the wild-type and the mutants, re-imported all Entrez lists were Venn mapped comparing each of the mutants to the wild-type (Figure 6A). This comparison showed that the number of altered genes in each mutant that did not overlap with those altered in the wild-type varied. The stop mutation Q368X contained the highest number of non-overlapping genes, both in absolute numbers and in percentage (2,247; 64%) (Figure 6A). The mutation R342K, whose absolute number of altered genes is the lowest of the mutants studied (Figure 2), contained 542 non overlapping genes, which amounts to a still high percentage of the total (56%) (Figure 6A). The other two mutants (set #2), D380N and K423E had a lower number of non-overlapping genes (24% and 22% respectively), sharing more of the changes with the wild-type.

To study the number of genes which were simultaneously altered in all mutants, we Venn mapped their FC ≥ 1.5 lists (Figure 6B). We found that a total of 73 genes were altered in all four mutants (Figure 6B).

Enriched Functions of the Mutant Overlapping Gene List

To investigate functions potentially involved in a common causative action of the four mutants studied, we searched for the GO enriched functions in the 73 mutant overlapping gene list. We analyzed the three GO SLIMS major functional categories of Biological Processes, Cellular Components and Molecular Functions, and sorted them by percent of genes in each of their

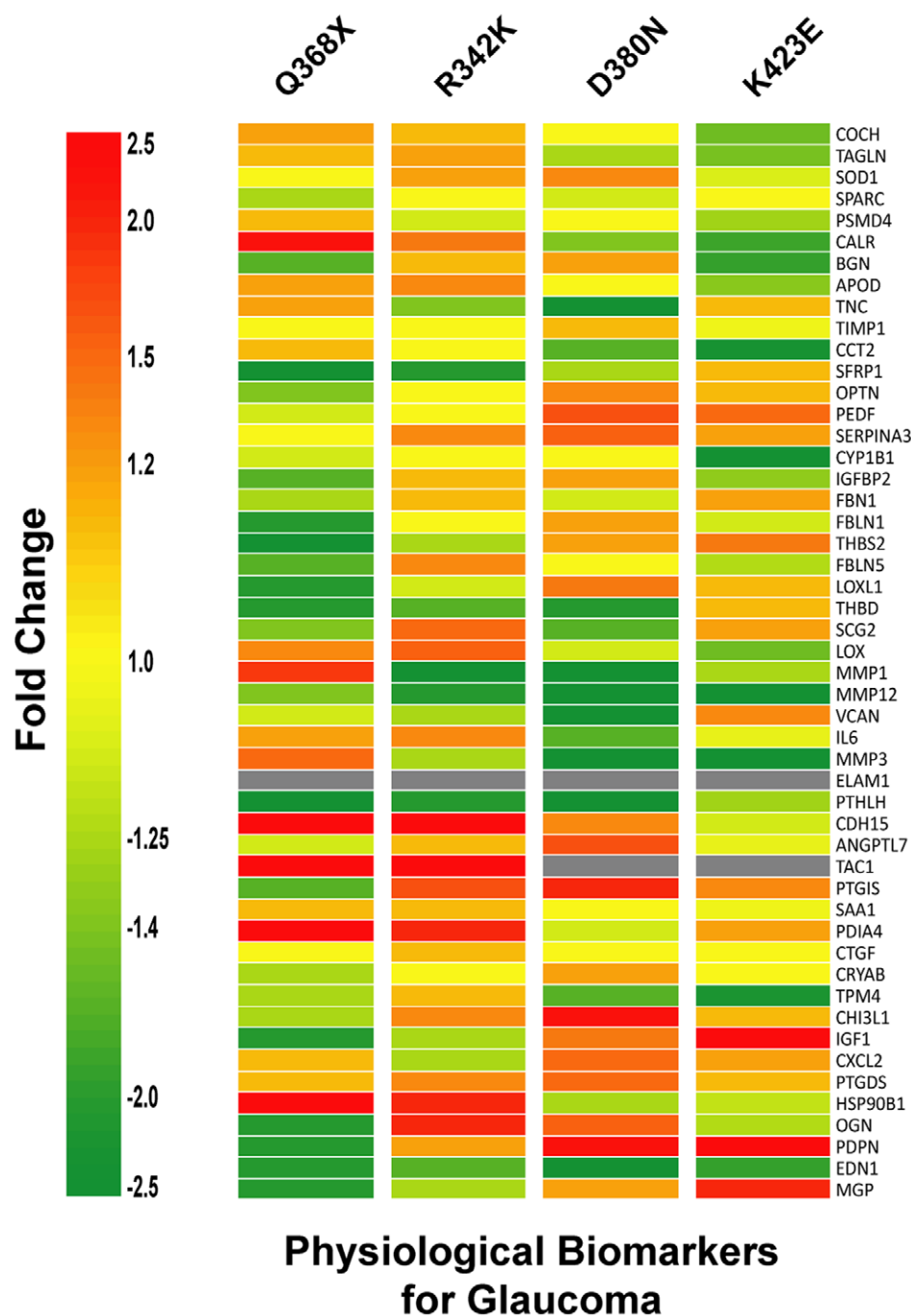


Figure 5. *MYOC* mutants altered most physiological biomarkers of glaucoma. Heat maps of a gene list containing 50 potential biomarkers for the human trabecular meshwork (Table S6). The biomarker gene list was generated by a comprehensive review of trabecular meshwork expression studies as indicated in the result section. Each row represents the fold change (Adeno.*MYOC* mutant over Adeno.Null) for a single gene in each of the four mutants. Each column represents the fold changes for all biomarkers in one *MYOC* mutant. The fold change for each gene is visually represented by a color, which is given by the scale bar at left. Heat maps were generated with genes lists containing the full range of fold changes. Gray cells indicate that the expression of the giving gene was below the cutoff of signal intensity value and was considered absent.
doi:10.1371/journal.pone.0036301.g005

subcategories which were statistically significant ($P \leq 0.05$). The diagram of the top seven subcategories from each main group is shown in Figure 7 top. In Biological Processes, cell cycle (GO:7049) contained the highest percent of genes number (23.1%, $P \leq 0.0003$), and DNA replication (GO:6260) was the most significant ($P \leq 0.000009$, 13.5% genes). In Cellular Components, the extracellular region subcategory (GO:5576) was both

the one with highest percentage of genes and most significant (25.9%, $P \leq 0.0001$). In the Molecular Function category, the subcategory with more genes was that of receptor binding (GO:5102) (15.8%, $P \leq 0.0009$) while the one most significant was the ATPase inhibitor activity (GO:42030) ($P \leq 0.00008$, 3.5% genes) (Figure 7 top).

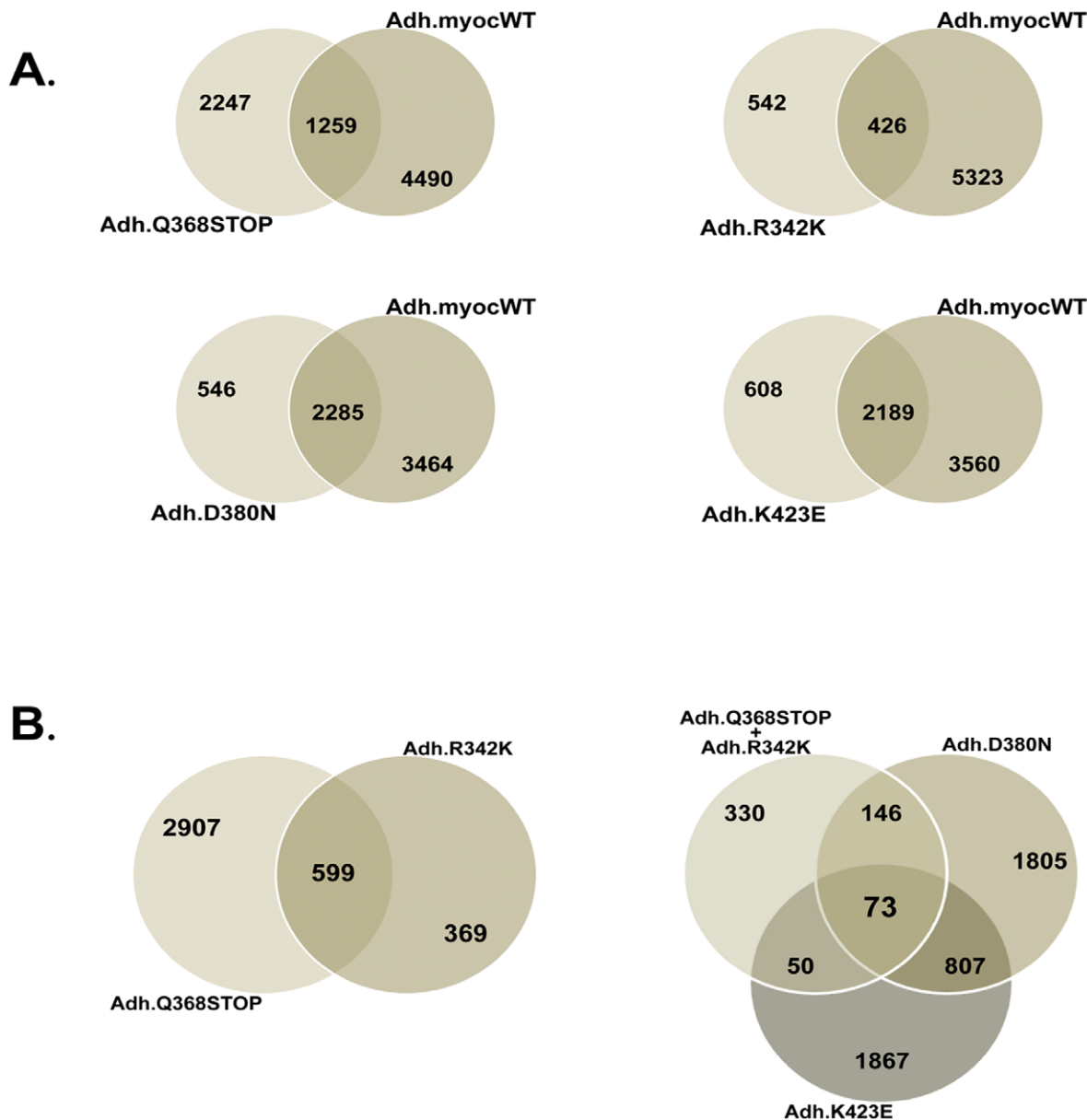


Figure 6. MYOC mutants shared different gene percentages with MYOC wild-type, and shared 73 genes among themselves. Venn diagrams of genes differentially altered 1.5-fold in response to overexpression of MYOC wild-type and MYOC-mutants. Each circle represents one condition. Intersections indicate numbers of genes that are shared between the different conditions. A) genes shared of each of the mutants with the wild-type. B) genes shared by all mutants.
doi:10.1371/journal.pone.0036301.g006

Genes selected from each of the lists of the subcategories are shown in Figure 7 lower panel. As expected, some of these genes coincide with those selected above through other selection means, ratifying the relevance of their potential involvement in the association of MYOC mutants with glaucoma. Among the genes, we observed the signaling cytokine *CXCL12*, the vasoconstrictor *EDN1*, the extracellular matrix constituent *ECM2*, the cysteine protease *CSTA*, the calcium homeostasis proteins *STC1*, *STC2* and the growth factors *IGF1* and *FGF1*. It is likely that a different extent combination of the functions encoded by these genes is what it would cause the MYOC mutants to trigger the development of the disease.

Genes Altered in All Mutants and not in the Wild-type. Identification of Cystatin A

Next we were interested to investigate whether the genes altered in all mutants were also altered in the wild-type. To determine how many of the 73 genes in the mutants' overlapping list were mutant-specific, we performed a Venn map comparing the shared mutant list with that of the 5,749 genes altered by the wild-type. Looking for non-overlapping genes, we found that only 10 out of the 73 genes were altered specifically in all mutants and were not shared with the altered genes of the wild-type (Figure 8).

Analysis of the functions of the 10 specific genes revealed the presence of a cysteine protease inhibitor, *CSTA* (alias *Stefin A*), which showed a no change 1.0-fold in the wild-type and an increase of 3.4-, 3.2-, 1.5- and 1.9-fold in Q368X, R342K, D380N

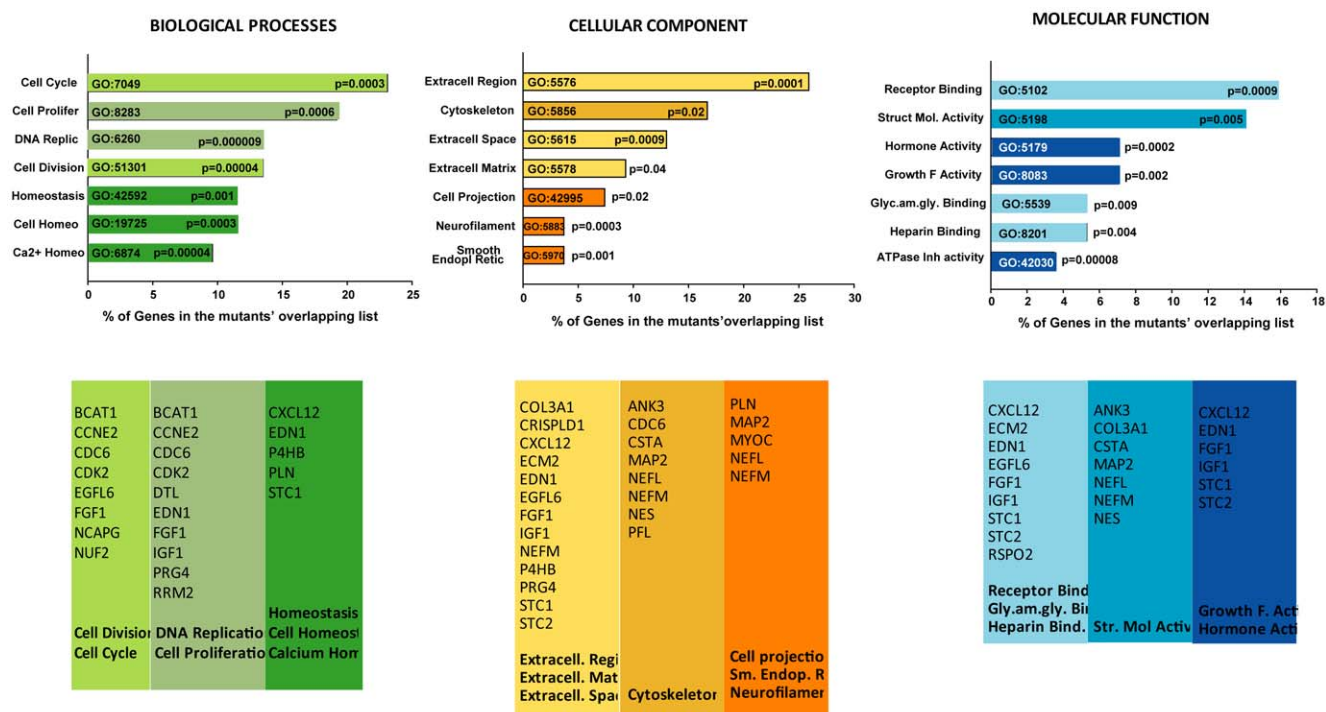


Figure 7. Gene ontology. The ECM category (GO:5576) contained the highest percent and significance of MYOC-induced genes. Top: enriched GO categories of the 73 gene list shared by all mutants (from Figure 6) sorted by *P* values. Bottom: genes selected from the categories shown on top (color coded). doi:10.1371/journal.pone.0036301.g007

and K423E respectively. The induction of *CSTA* in all cells overexpressing the MYOC mutants was validated by TaqMan PCR in a different HTM primary cell line (HTM-137) and using new viral stocks. Cells were infected with each of the four mutants, Ad5.CMV-Null and Adh.MYOCWT as indicated in methods. RNA was extracted 48 h post-infection and its cDNA assayed for expression of *CSTA*, using *MYOC* as a positive control and 18S as the endogenous calibrator. Results were expressed in FC values of each of the genes in the treated (MYOCs) over negative control (Ad5.CMV.Null), and normalized to their own 18S. In cells infected with Q368X, R342K, D380N and K423E, *CSTA* was induced 4.6-fold ($P = 0.012$), 3.7-fold ($P = .001$), 6.45-fold ($p = 0.015$), and 5.7-fold ($P = 0.002$) respectively. In cells infected with Adh.MYOCWT, rather than a no change as it occurred in the chip, *CSTA* was reduced -3.0 -fold ($P = 0.0001$), a result most likely due to the highest sensitivity to the TaqMan assay. The overexpression of *MYOC* in each of the dishes (mutants and wild-type infected) was used as a positive control and ranged from 891 to 7,131 FC over that in Ad5.CMV-Null.

Functional Assay of Cystatin A. Involvement in Wild-type Myocilin Processing

In order to investigate whether overexpression of the selected *CSTA* gene would affect the processing of the wild-type *MYOC* protein we generated tagged recombinant plasmids, containing both genes (Figure 9A). Plasmid pMG29 contains 1513 nt of wild-type *MYOC* fused to the V5 tag in a pCDNA3.1D V5-His-TOPO background. Plasmid pCSTA contains the full coding *CSTA* cDNA (Origene) fused to the DDK and MYC elements. Plasmid pCSTAm derives from pCSTA but contains a mutation at nucleotide 139 (G to A) that converts N-terminal Gly-4 residue to an Arginine and inactivates the binding of the inhibitor to the

cathepsin B protease [37]. Plasmid pEmpty does not contain any transgene cDNA (see methods) and was used as a control. pMG29 was co-transfected with either pCSTA or pEmpty in HEK293 and primary HTM-137 cells in a ratio of 1:2 (Figures. 9B and 9C). Extracted intracellular and secreted proteins were run in PAGE gels, blotted and cross-reacted with an antibody against the V5 tag fused to MYOC. Blots were then re-probed with beta-actin for equal loading control and with anti-DDK antibody to confirm the presence of *CSTA*. The 35 K processed C-terminal appeared as a doublet. In both cell lines, the processing of the wild-type was reduced in the presence of the *CSTA* protein.

In the HEK293 cells secreted fraction, densitometry of the wild-type and processed C-terminal fragments showed a mean density of the processed MYOC bands to be a 48.6% of the total secreted MYOC in the cells transfected with pEmpty and 36.4% in the cells transfected with pCSTA (a percent reduction of 25.1%). The difference was more marked in the intracellular fraction where the processed MYOC was 49.8% of the total in the control and 12.5% in the cells transfected with *CSTA* (a percent reduction of 74.9%).

In the primary HTM cells secreted fraction, densitometry of the wild-type and processed C-terminal fragments bands showed the mean density of the processed MYOC to be 33.0% of the total secreted MYOC in the cells transfected with pEmpty controls and 17.2% in the cells transfected with pCSTA (a percent reduction of 47.9%). The difference was more marked in the intracellular fraction where the processed MYOC was 36.5% of the total in the control and 6.6% in the cells transfected with *CSTA* (percent reduction of 89.1%). Protein extracts were run in duplicate gels and transfections were repeated on the HEK293 to confirm the findings. Confirmation of the processing effect of *CSTA* in wild-type MYOC was achieved by the transfection and overexpression of HTM-137 cells with pCSTAm, a plasmid where the activity of

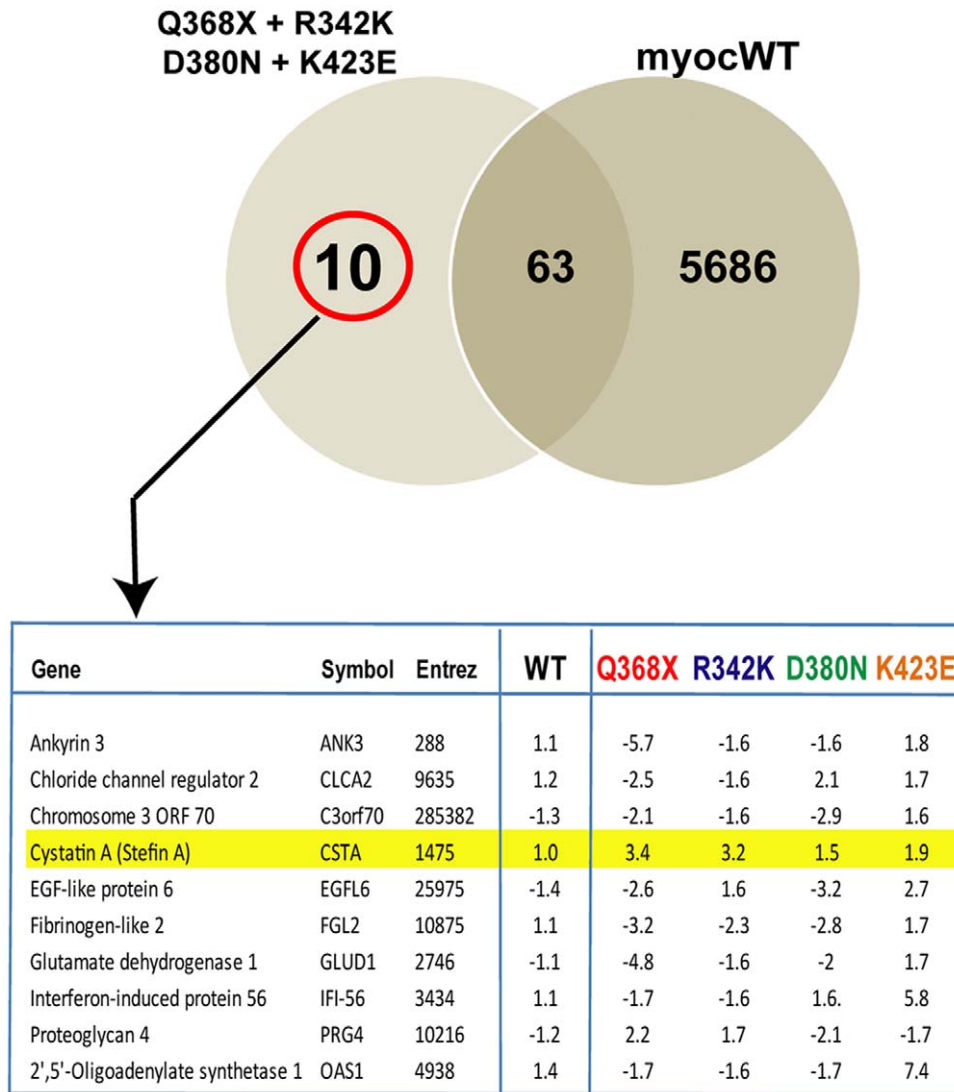


Figure 8. Cystatin A is induced in all *MYOC* mutants and not in *MYOC* wild-type. Top: Venn diagram comparing genes altered 1.5-fold in all *MYOC* mutants (left circle) with those altered in the *MYOC* wild-type (right circle) (from Figure 6). Intersection indicates numbers of altered genes which are shared between all the mutants and those altered in the wild-type. Number of genes specifically altered by the mutants is outside the intersection and circled in red. Bottom: list of specific genes highlighting Cystatin A and its altered fold change values in each condition. doi:10.1371/journal.pone.0036301.g008

the CSTA protein is destroyed by the mutation of the conserved residue Gly-4 to Arg [37] (Figure 9D). In the secreted fraction, densitometry readings of the mutant experiments showed the processed MYOC in cells transfected with pEmpty and pCSTAm to be 23.6% and 37.1% respectively of the total secreted, while in cells transfected with pCSTA was 10.5% (percent reductions of 55.5 and 71.7% respectively). In the intracellular fraction, the processed MYOC was 17.2% and 20.4% of the total MYOC in cells transfected with pEmpty and pCSTAm and 9.5% in cells transfected with pCSTA (percent reductions of 44.8% and 53.4% respectively).

These results indicate that the increased levels of the protease inhibitor CSTA, but not those of the inactivated CSTA, are able to inhibit the processing of MYOC. In both cell types the inhibition occurred in both fractions and the reduction seems to be higher in the non-transformed trabecular meshwork specific cells than in the transformed embryonic kidney HEK293 line. Therefore the previously reported protein processing reduction

observed in the *MYOC* mutants [28] might be due to overexpression of *CSTA*. The finding could lead to a common treatment of the inhibition of *CSTA* to ameliorate the development of the disease caused by *MYOC* mutants.

Discussion

Our goal in this study was to gain insight into the molecular mechanisms linking *MYOC* mutants to the development of glaucoma. Even if the *MYOC* gene is expressed in several non-ocular tissues, *MYOC* mutants are associated to only one disease, glaucoma. Because myocilin is induced by a variety of stress factors (from oxidative stress to mechanical strain), it is very likely that the disease caused by the *MYOC* mutants would be aggravated by their induced overexpression under stress conditions. To date, a few studies have addressed the effect of overexpressing some *MYOC* mutants in ocular and non-ocular cells [15,18,23,28]. However, except for one study in fruit flies [19], most of them

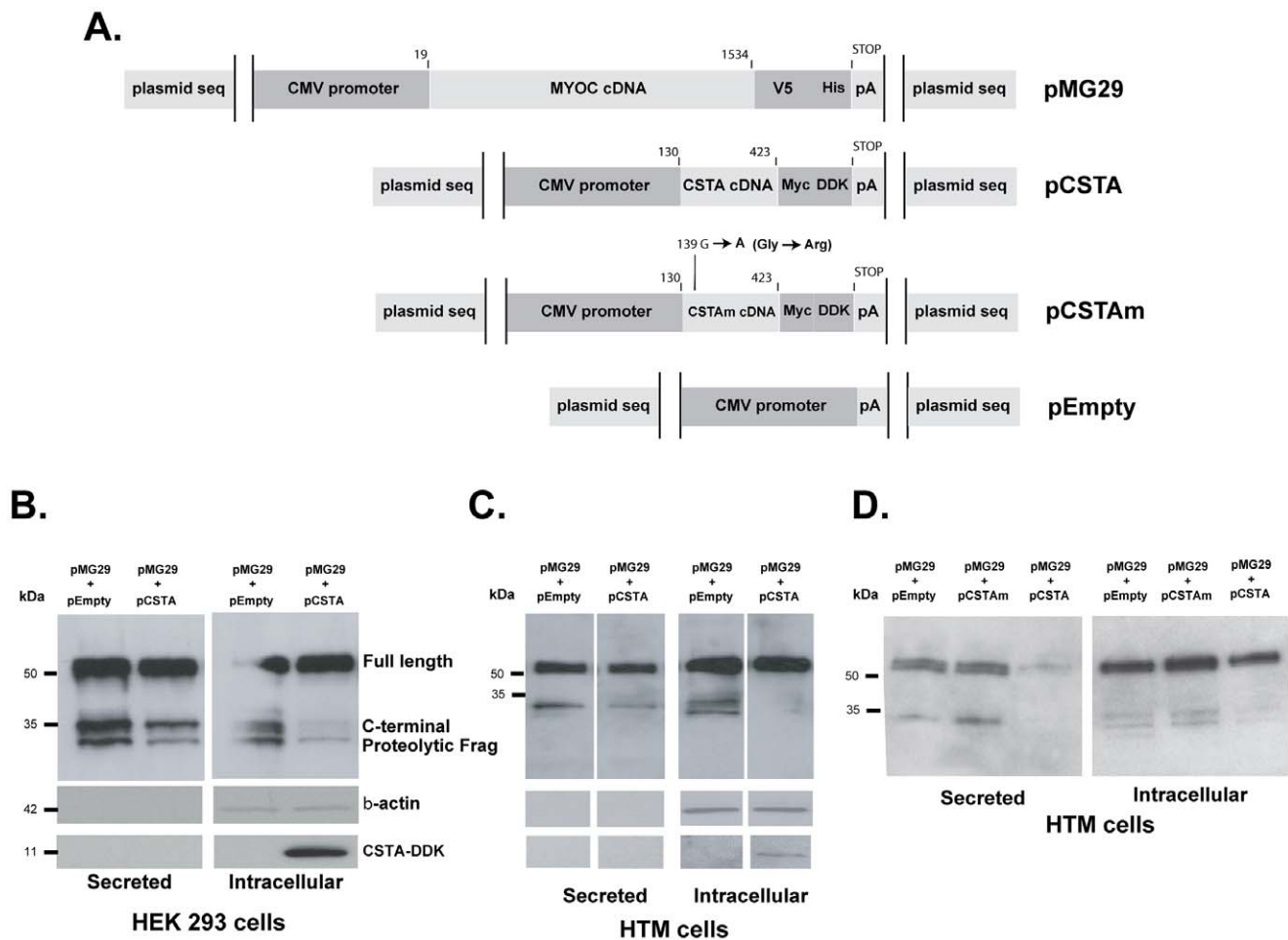


Figure 9. Cystatin A inhibits the processing of MYOC wild-type in cultured cells. Recombinant expression plasmids containing tag-fused full coding wild-type *MYOC* (pMG29), *CSTA*, and controls plasmids, inactive mutated *CSTA* (*CSTAm*) and pEmpty, were generated as indicated in Methods. pMG29 was co-transfected with either pCSTA, pCSTAm or pEmpty (1:2) and harvested at 48 h post-transfection. Equivalent volumes of cell extracts and of their supernatants were loaded onto 4–15% SDS-PAGE gels, transferred to PVDF membranes and analyzed by immunoblotting. Different *MYOC* protein forms (full length and processed) were detected with an anti-V5 mouse monoclonal followed by an anti-mouse horseradish peroxidase antibodies. Blots were re-probed with β -actin and DDK antibodies for loading and identification controls. Percent of the *MYOC* processed band was calculated by densitometry. A) schematic representation of the expression cassettes of the recombinant plasmids. B, C and D: Representative western blots with extracts from transfected cells. B) extracts from HEK293 co-transfected by calcium phosphate. C and D) extracts from primary HTM-137 cells co-transfected by nucleofactor electroporation.

doi:10.1371/journal.pone.0036301.g009

focused on the effect of the mutants in a few cellular mechanisms. Because *MYOC* mutants cause high tension glaucoma in humans, and because an elevated IOP phenotype is the result of a dysfunctional trabecular meshwork, here we studied the effect of overexpressing them in primary non-transformed, human trabecular meshwork cells. With the intent of uncovering new mechanisms, our approach entailed the examination of global changes induced by the mutants in the entire transcriptome of the cell.

Genes, known and New

When we examined the most altered genes induced by all four mutants, we observed a high number of genes which had been previously identified as functionally relevant for the trabecular meshwork at either physiological or glaucomatous stress conditions. Among those genes are *EDN1*, *MGP*, *IGF1*, *CALR*, *PDI4*, *PCLOCE2*, *MMP1*, *MMP3*, *SFRP1*, *FN1*, *PDPN*, *OGN*, *OSF2*, *THBS2*, *THBD*, *LOX*, *LOX-L1*, *TAC1*, *Secretogranin II (SCG2)* and *SNCA*. Some of these had already been reported to be associated

with *MYOC* mutants (e.g. *MMP1*, *CALR*, and *PDI*) or wild-type (*SFRP1*, *FN1*) in other studies [18,19,41] [25,63], and validates the finding. However, the association of most of them with *MYOC* mutants was unknown.

As is not uncommon in this type of studies, some of the found genes appeared to serve a counteracting purpose while others appeared to be directly related to the detrimental effect. For example, *END1* was on the top downregulated list in all four mutants. Endothelin protein is processed to secrete a potent vasoconstrictor peptide with a well-established connection to glaucoma [64]. Endothelin can lower IOP by contracting the ciliary muscle, but conversely, an antagonist of its receptor can also lower IOP in glaucomatous monkeys [64]. The endogenous *EDN1* downregulation by myocilin mutants seen here is curious. It could be interpreted as either a signal for contributing to the high IOP phenotype of the mutants or to a counteracting effect.

A gene that could enlighten the correlation between the mutants and elevated IOP is *MMP1*. In this study all mutants but one (Q368X) downregulated *MMP1*, while the wild-type upregulated

its expression. Matrix metalloproteinase 1 breaks down collagen type 1, an important component of the ECM of the outflow tissue. Increased levels of *MMP1* have been extensively associated with increasing outflow facility and lowering of IOP [41,65]. Therefore, the *MMP1* downregulation observed here could be seen as a contribution to the build-up of an ECM excess, increase of aqueous humor resistance and consequent elevated IOP produced by the mutants. The unexpected upregulation of *MMP1* by Q368X (confirmed repeatedly by TaqMan PCR) could then be explained as one of the molecular reasons as to why this mutation causes a milder outcome of the disease. Curiously, we had previously reported an interesting feedback loop regulation of expression between the *MMP1*/*MYOC* genes [31,41,66], where overexpression of wild-type *MYOC* induced the expression of *MMP1* [31] while overexpression of *MMP1* reduced that of wild-type *MYOC* [41,66]. It is possible that a homeostatic balance between these two proteins would be disrupted by the presence of the mutated protein form.

Another potentially relevant gene found in these studies was *PDIA4*. In an earlier report overexpressing Q368X in trabecular meshwork cells, Kee and co-workers [18] had observed increased PDI levels in the treated cells. In this study *PDIA4* expression was induced by both the Q368X and R342K mutants, but not by D380N and K423E. This enzyme which catalyzes the formation and breakage of disulfide bonds is a key component of the protein folding mechanism. Myocilin folding and complex formation is relevant for its function and has been known to be mediated by the formation of covalent disulfide bonds involving its five cysteine residues [67]. Although the fifth residue 433Cys is not present in the Q368X stop mutation, the induction of the PDI is bound to affect the stability of the proteins and even perhaps affect the secretion of other proteins [68]. In our early work, *PDIA4* was induced in response to elevated pressure [45,46]. It is known that mechanical strain causes deformation of proteins, triggering them to unfold and subsequently refold [69]. Protein disulfide isomerase induction could thus be a mediator of this effect and represent a cellular defense response against the altered protein, as it also occurs in Creutzfeldt-Jacob disease [70]. Why *PDIA4* is only induced by two of the mutants is not yet clear and might be a sign of the different avenues through which each mutant contributes to the disease.

Some of the genes altered by these mutants were new. These include among others *RAB39B*, *STC1*, *CDH15*, *CXCL12*, *CSTA*, *ECM2* and *Lysosomal-associated membrane protein 3 (LAMP3)*, a gene which is expressed in lymphoid organs and dendritic cells. Some of these genes were commonly altered in all mutants while others where changed only in one or two of them. Their encoded functions could play a role on the mutant's linkage to the disease. Thus, *RAB39B*, upregulated in all mutants, is a small GTPase binding protein described as being specific to neurons and involved in vesicular trafficking [71]. This mechanism, which includes the ability to secrete the protein, has been shown to play a key role in myocilin function [12,13] and was suggested to be disrupted by *MYOC* mutants [11]. It would be possible that upregulation of *RAB39B* could have a role on the trafficking and non-secretion of the *MYOC* mutants.

Another new gene, *STC1*, was in contrast downregulated in all mutants. Stanniocalcin regulates calcium and phosphate transport in the kidney and has been postulated to prevent hypercalcemia [72]. The downregulation of *STC1* could be an indication that the *MYOC* mutants are favoring a trend towards calcification of the trabecular meshwork.

Few of the genes encoding proteins reported to interact with Myocilin made the 1.5X FC cutoff. Two of them did. Secreted

frizzled protein 1, [25] which was downregulated in mutants Q368X and R342K, and *EN1* [63], that was upregulated in D380N and K423E. The *SNCA* gene which was also upregulated in D380N and K423E is from the same family as the *MYOC* binding protein γ -synuclein, but in contrast, showed no colocalization and thus, not binding [73]. α -Synuclein, is a protein abundant in neurons and involved in Parkinson and other neurodegenerative disorders and in here could play the role of a pathological chaperone, as it has been described in other systems [74]. α -Synuclein peptides are a major component of amyloid plaques in the brains of patients with Alzheimer's disease [75], which has been speculated to have some common mechanistic features with Glaucoma [76].

Differences between Mutants

Overall, there were many similarities between Q368X and R342K (which we termed set #1). Those similarities were distinct from the changes induced by the other two mutants D380N and K423E (set #2). This was an unexpected finding, since there are not described phenotypic similarities shared between the mutants of the same group, or described phenotypic differences between the two groups. At the moment we can postulate that, in addition to IOP, there may yet be undefined glaucoma biomarkers in the altered genes pool which could differently influence the development of the disease in sets #1 and #2.

A look at the genes representing trabecular meshwork relevant functions and physiological markers of glaucoma by the use of heat maps (Figures 4 and 5) revealed that most of genes in those lists are affected by overexpression of *MYOC* mutants. The trend of similarities between the two sets of mutants is clearly seen in the genes involved in calcification, WNT signaling and stress, while it is less obvious in those genes encoding collagen-elastic cross-linking and in the biomarkers' list. The intensity of the changes was considerably greater in the stress and UPR function group, especially for the Q368X mutation. This mutation clearly downregulated genes that could induce elevated IOP, such *TGM2* and *SFRP1* [26,60] while inducing others that have a role in protein folding, such as *CALR* and *Calnexin (CANX)*. This combined regulation could be beneficial and contribute to the milder outcome of the disease in the Q368X mutant. In contrast, the lower induction of the same genes (*CALR* and *CANX*) by R342K, together with the upregulation of the calcification genes *OGN* and *OMD* (heat map Figure 4) could provide this mutant (otherwise similar to the stop mutation) with the difference needed to induce an elevated pressure.

Although each of the *MYOC* mutants exhibited individual characteristics which are most likely instrumental in triggering different disease severities, there was a need to search for a common thread. In a Venn map comparison with wild-type we observed that the four *MYOC* mutants exhibited a different percentage of non-shared altered genes. Set #1 mutants had a larger non-shared percentage than set #2. This could be an indication that set #1 would be further away from the proposed protective mechanism of the wild-type than set #2 or, that these mutants require a higher number of changes to cause the disease. When comparing the four mutants against themselves, we found only 73 altered common genes. And from the 73, only 10 were not altered in the wild-type.

Cystatin A as a Potential Common Link

One of the genes found elevated in all mutants and not elevated in the wild-type was *CSTA*, which encodes for the cysteine protease inhibitor cystatin A. This gene is present in most tissues, its expression is associated with tumor growth and it is a serum

biomarker for screening cancer patients. The upregulation of the *CSTA* mRNA by the *MYOC* mutants is intriguing. Because the protein involved in the processing of myocilin, calpain II, is a cysteine protease, and because myocilin cleavage is inhibited by *MYOC* mutants, one could reasonably infer that *CSTA* plays a role in the inhibition of the process. Whether the elevation of cystatin A seen here can result also in the inhibition of calpain is not yet known. Cystatin A is known to inhibit papain and cathepsins, not calpains. However, a recent study investigating induced cell death in monocytes and macrophages has shown that calpain activation occurred downstream of cathepsin B (a *CSTA* substrate) [77]. They concluded that cathepsin B activated calpain [77]. Such finding would implicate that increased levels of cystatin A would, by inactivating cathepsin B, result in the inactivation of calpain. In our functional assay, overexpression of cystatin A reduced the processing of wild-type myocilin while overexpression of an inactive *CSTA* did not. This effect could then have been achieved by either a downstream inactivation of calpain through the inactivation of cathepsin B, or by a direct cleavage of myocilin by cathepsin B.

It is important to point out that *MYOC*-causative glaucoma occurs only in heterozygous individuals, and that *MYOC* forms wild-type/mutant hetero-oligomers which lead to the formation of insoluble aggregates (gain of function) [12,17]. It would be logical to assume that myocilin processing, affected by the expression of the mutants, plays a fundamental role in the formation of the hetero-aggregates. The fact that hetero-aggregation could also modulate the extracellular environment [15] provides an additional support for the relevance of faulty hetero-aggregates in the development of glaucoma.

Finally, although several mechanisms are bound to be involved in the association of *MYOC* mutants to glaucoma, it looks that activation of cysteine protease inhibitors could be a common, general one. It would be interesting to investigate whether the application of an inhibitor to *CSTA*, such as its siRNA, could restore the normal *MYOC* processing and affect the outcome of the disease. Our results showing that overexpression of an inactive *CSTA* reverted the decrease processing would support this possibility. It would also be of interest to determine whether a screening of *CSTA* levels in the serum could be applied to glaucoma as it is presently occurring in cancer [39].

Conclusions

Our study on the transcripts altered by overexpression of *MYOC* mutants in glaucoma-relevant primary human cells provides key insights on the potential mechanisms leading to the development of *MYOC*-linked glaucoma. We uncovered that each mutant's phenotype could result from its unique effect on the transcriptome. We learned that a number of important genes which have been historically associated with physiological and pathological mech-

anisms of the human trabecular meshwork are altered by the expression of these *MYOC* mutants. On overall mechanisms, we identified that, genes of the UPR pathway were the most affected. On individual gene analyses, we confirmed the involvement of previously *MYOC*-associated genes (e.g. *MMP1*, *PDIA4*, *CALR*, *SEPR1*) and revealed the relevance of some new ones (e.g. *STC1*, *RAB39B*, *CXCL12*). Most importantly, we discovered a mutant-specific induced gene, *CSTA*. This inhibitor of cysteine proteases was functional, and inhibited *MYOC* protein processing in cultured cells. We believe these findings do significantly impact our understanding of *MYOC*-caused glaucoma and could provide the basis for the potential development of a broad-spectrum therapy for the mutant disease.

Supporting Information

Table S1 Q368STOP. The 100 most altered genes. a) 50 upregulated; b) 50 downregulated (XLSX)

Table S2 R342K. The 100 most altered genes. a) 50 upregulated; b) 50 downregulated (XLSX)

Table S3 D380N. The 100 most altered genes. a) 50 upregulated; b) 50 downregulated (XLSX)

Table S4 K423E. The 100 most altered genes a) 50 upregulated; b) 50 downregulated (XLSX)

Table S5 Taqman FC and p-values of selected relevant genes. Comparison to microarray FC (XLSX)

Table S6 Physiological Biomarkers List for Glaucoma (Trabecular Meshwork). (XLSX)

Acknowledgments

The authors thank Drs. M.A. Carbone and R.R.H. Anholt for providing the myocilin mutant plasmids. They also thank members of the laboratory, Dr. M.G. Spiga for generating the fusion myocilin clone, M.H. Smith and R. Elliott for generation of the gene tables and Dr. J. Carabaña for critical reading of the manuscript.

Author Contributions

Conceived and designed the experiments: TB KDK SAA. Performed the experiments: KDK SAA LKKB. Analyzed the data: TB KDK SAA. Contributed reagents/materials/analysis tools: KDK SAA LKKB. Wrote the paper: TB KDK.

References

- Polansky JR, Kurtz RM, Fauss DJ, Kim RY, Bloom E (1991) *In vitro* correlates of glucocorticoid effects on intraocular pressure. In: Kriegstein GK, ed. Glaucoma Update IV. Berlin, Heilderberg: Springer-Verlag. pp 20–29.
- Escribano J, Ortego J, Coca-Prados M (1995) Isolation and characterization of cell-specific cDNA clones from a subtractive library of the ocular ciliary body of a single normal human donor: transcription and synthesis of plasma proteins. *J Biochem* 118: 921–931.
- Kubota R, Noda S, Wang Y, Minoshima S, Asakawa S, et al. (1997) A novel myosin-like protein (myocilin) expressed in the connecting cilium of the photoreceptor: molecular cloning, tissue expression, and chromosomal mapping. *Genomics* 41: 360–369.
- Ortego J, Escribano J, Coca-Prados M (1997) Cloning and characterization of subtracted cDNAs from a human ciliary body library encoding TIGR, a protein involved in juvenile open angle glaucoma with homology to myosin and olfactomedin. *FEBS Lett* 413: 349–353.
- Lo WR, Rowlette LL, Caballero M, Yang P, Hernandez MR, et al. (2003) Tissue differential microarray analysis of dexamethasone induction reveals potential mechanisms of steroid glaucoma. *Invest Ophthalmol Vis Sci* 44: 473–485.
- Stone EM, Fingert JH, Alward WL, Nguyen TD, Polansky JR, et al. (1997) Identification of a gene that causes primary open angle glaucoma. *Science* 275: 668–670.
- Shimizu S, Lichter PR, Johnson AT, Zhou Z, Higashi M, et al. (2000) Age-dependent prevalence of mutations at the GLC1A locus in primary open-angle glaucoma. *Am J Ophthalmol* 130: 165–177.
- Quigley HA, Broman AT (2006) The number of people with glaucoma worldwide in 2010 and 2020. *Br J Ophthalmol* 90: 262–267.
- Gong G, Kosoko-Lasaki O, Haynatzki GR, Wilson MR (2004) Genetic dissection of myocilin glaucoma. *Hum Mol Genet* 13 Spec No 1: R91–102.

10. Nguyen TD, Chen P, Huang WD, Chen H, Johnson D, et al. (1998) Gene structure and properties of TIGR, an olfactomedin-related glycoprotein cloned from glucocorticoid-induced trabecular meshwork cells. *J Biol Chem* 273: 6341–6350.
11. Caballero M, Borrás T (2001) Inefficient processing of an olfactomedin-deficient myocilin mutant: potential physiological relevance to glaucoma. *Biochem Biophys Res Commun* 282: 662–670.
12. Caballero M, Rowlette LL, Borrás T (2000) Altered secretion of a TIGR/MYOC mutant lacking the olfactomedin domain. *Biochim Biophys Acta* 1502: 447–460.
13. Perkumas KM, Hoffman EA, McKay BS, Allingham RR, Stamer WD (2007) Myocilin-associated exosomes in human ocular samples. *Exp Eye Res* 84: 209–212.
14. Jacobson N, Andrews M, Shepard AR, Nishimura D, Searby C, et al. (2001) Non-secretion of mutant proteins of the glaucoma gene myocilin in cultured trabecular meshwork cells and in aqueous humor. *Hum Mol Genet* 10: 117–125.
15. Aroca-Aguilar JD, Sanchez-Sanchez F, Martinez-Redondo F, Coca-Prados M, Escribano J (2008) Heterozygous expression of myocilin glaucoma mutants increases secretion of the mutant forms and reduces extracellular processed myocilin. *Mol Vis* 14: 2097–2108.
16. Zhou Z, Vollrath D (1999) A cellular assay distinguishes normal and mutant TIGR/myocilin protein. *Hum Mol Genet* 8: 2221–2228.
17. Gobeil S, Rodrigue MA, Moisan S, Nguyen TD, Polansky JR, et al. (2004) Intracellular sequestration of hetero-oligomers formed by wild-type and glaucoma-causing myocilin mutants. *Invest Ophthalmol Vis Sci* 45: 3560–3567.
18. Joe MK, Sohn S, Hur W, Moon Y, Choi YR, et al. (2003) Accumulation of mutant myocilins in ER leads to ER stress and potential cytotoxicity in human trabecular meshwork cells. *Biochem Biophys Res Commun* 312: 592–600.
19. Carbone MA, Ayroles JF, Yamamoto A, Morozova TV, West SA, et al. (2009) Overexpression of myocilin in the *Drosophila* eye activates the unfolded protein response: implications for glaucoma. *PLoS One* 4: e4216.
20. Morissette J, Clepet C, Moisan S, Dubois S, Winstall E, et al. (1998) Homozygotes carrying an autosomal dominant TIGR mutation do not manifest glaucoma. *Nat Genet* 19: 319–321.
21. Tamm ER (2002) Myocilin and glaucoma: facts and ideas. *Prog Retin Eye Res* 21: 395–428.
22. Comes N, Borrás T (2009) Individual molecular response to elevated intraocular pressure in perfused postmortem human eyes. *Physiol Genomics* 38: 205–225.
23. Joe MK, Tomarev SI (2010) Expression of myocilin mutants sensitizes cells to oxidative stress-induced apoptosis: implication for glaucoma pathogenesis. *Am J Pathol* 176: 2880–2890.
24. Mena F, Braghini CA, Vasconcellos JP, Mena B, Costa VP, et al. (2011) Keeping an eye on myocilin: a complex molecule associated with primary open-angle glaucoma susceptibility. *Molecules* 16: 5402–5421.
25. Kwon HS, Lee HS, Ji Y, Rubin JS, Tomarev SI (2009) Myocilin is a modulator of Wnt signaling. *Mol Cell Biol* 29: 2139–2154.
26. Wang WH, McNatt LG, Pang IH, Millar JC, Hellberg PE, et al. (2008) Increased expression of the WNT antagonist sFRP-1 in glaucoma elevates intraocular pressure. *J Clin Invest* 118: 1056–1064.
27. Goldwich A, Ethier CR, Chan DW, Tamm ER (2003) Perfusion with the olfactomedin domain of myocilin does not affect outflow facility. *Invest Ophthalmol Vis Sci* 44: 1953–1961.
28. Aroca-Aguilar JD, Sanchez-Sanchez F, Ghosh S, Coca-Prados M, Escribano J (2005) Myocilin mutations causing glaucoma inhibit the intracellular endoproteolytic cleavage of myocilin between amino acids Arg226 and Ile227. *J Biol Chem* 280: 21043–21051.
29. Aroca-Aguilar JD, Martinez-Redondo F, Sanchez-Sanchez F, Coca-Prados M, Escribano J (2010) Functional role of proteolytic processing of recombinant myocilin in self-aggregation. *Invest Ophthalmol Vis Sci* 51: 72–78.
30. Sanchez-Sanchez F, Martinez-Redondo F, Aroca-Aguilar JD, Coca-Prados M, Escribano J (2007) Characterization of the intracellular proteolytic cleavage of myocilin and identification of calpain II as a myocilin-processing protease. *J Biol Chem* 282: 27810–27824.
31. Borrás T, Bryant PA, Chisolm SS (2006) First look at the effect of overexpression of TIGR/MYOC on the transcriptome of the human trabecular meshwork. *Exp Eye Res* 82: 1002–1010.
32. Challa P, Herndon LW, Hauser MA, Broomer BW, Pericak-Vance MA, et al. (2002) Prevalence of myocilin mutations in adults with primary open-angle glaucoma in Ghana, West Africa. *J Glaucoma* 11: 416–420.
33. Wirtz MK, Samples JR, Choi D, Gaudette ND (2007) Clinical features associated with an Asp380His Myocilin mutation in a US family with primary open-angle glaucoma. *Am J Ophthalmol* 144: 75–80.
34. Brutti M, Longo I, Frezzotti P, Ciappetta R, Randazzo A, et al. (2003) Mutations in the myocilin gene in families with primary open-angle glaucoma and juvenile open-angle glaucoma. *Arch Ophthalmol* 121: 1034–1038.
35. Rivenbark AG, Coleman WB (2009) Epigenetic regulation of cystatins in cancer. *Front Biosci* 14: 453–462.
36. Martin JR, Craven CJ, Jerala R, Kroon-Zitko L, Zerovnik E, et al. (1995) The three-dimensional solution structure of human stefin A. *J Mol Biol* 246: 331–343.
37. Estrada S, Nycander M, Hill NJ, Craven CJ, Walther JP, et al. (1998) The role of Gly-4 of human cystatin A (stefin A) in the binding of target proteinases. Characterization by kinetic and equilibrium methods of the interactions of cystatin A Gly-4 mutants with papain, cathepsin B, and cathepsin L. *Biochemistry* 37: 7551–7560.
38. Blaydon DC, Nitoiu D, Eckl KM, Cabral RM, Bland P, et al. (2011) Mutations in CSTA, encoding Cystatin A, underlie exfoliative ichthyosis and reveal a role for this protease inhibitor in cell-cell adhesion. *Am J Hum Genet* 89: 564–571.
39. Chang KP, Wu CC, Chen HC, Chen SJ, Peng PH, et al. (2010) Identification of candidate nasopharyngeal carcinoma serum biomarkers by cancer cell secretome and tissue transcriptome analysis: potential usage of cystatin A for predicting nodal stage and poor prognosis. *Proteomics* 10: 2644–2660.
40. He TC, Zhou S, da Costa LT, Yu J, Kinzler KW, et al. (1998) A simplified system for generating recombinant adenoviruses. *Proc Natl Acad Sci U S A* 95: 2509–2514.
41. Spiga MG, Borrás T (2010) Development of a gene therapy virus with a glucocorticoid-inducible MMP1 for the treatment of steroid glaucoma. *Invest Ophthalmol Vis Sci* 51: 3029–3041.
42. Comes N, Buie LK, Borrás T (2011) Evidence for a role of angiopoietin-like 7 (ANGPTL7) in extracellular matrix formation of the human trabecular meshwork: implications for glaucoma. *Genes Cells* 16: 243–259.
43. Thorleifsson G, Magnusson KP, Sulem P, Walters GB, Gudbjartsson DF, et al. (2007) Common sequence variants in the LOXL1 gene confer susceptibility to exfoliation glaucoma. *Science* 317: 1397–1400.
44. Borrás T (2008) Mechanosensitive genes in the trabecular meshwork at homeostasis: elevated intraocular pressure and stretch. In: Tombran-Tink J, Barnstable CJ, Shields MB, eds. *Mechanisms of the Glaucomas: Disease Processes and Therapeutic Modalities*. New York: Humana Press, Inc. pp 329–362.
45. Borrás T (2008) What is Functional Genomics teaching us about intraocular pressure regulation and glaucoma? In: Civan MM, ed. *The Eye's Aqueous Humor*, Second Edition. San Diego: Elsevier. pp 323–377.
46. Vittitow J, Borrás T (2004) Genes expressed in the human trabecular meshwork during pressure-induced homeostatic response. *J Cell Physiol* 201: 126–137.
47. Xu H, Acott TS, Wirtz MK (2000) Identification and expression of a novel type I procollagen C-proteinase enhancer protein gene from the glaucoma candidate region on 3q21-q24. *Genomics* 66: 264–273.
48. Stoilov I, Akarsu AN, Sarfarazi M (1997) Identification of three different truncating mutations in cytochrome P4501B1 (CYP1B1) as the principal cause of primary congenital glaucoma (Buphthalmos) in families linked to the GLC3A locus on chromosome 2p21. *Hum Mol Genet* 6: 641–647.
49. Gonzalez P, Epstein DL, Borrás T (2000) Genes upregulated in the human trabecular meshwork in response to elevated intraocular pressure. *Invest Ophthalmol Vis Sci* 41: 352–361.
50. Borrás T, Comes N (2009) Evidence for a calcification process in the trabecular meshwork. *Exp Eye Res* 88: 738–746.
51. Schlötzer-Schrehardt U (2009) Molecular pathology of pseudoexfoliation syndrome/glaucoma—new insights from LOXL1 gene associations. *Exp Eye Res* 88: 776–785.
52. Gonzalez P, Epstein DL, Borrás T (2000) Characterization of gene expression in human trabecular meshwork using single-pass sequencing of 1060 clones. *Invest Ophthalmol Vis Sci* 41: 3678–3693.
53. Tomarev SI, Wistow G, Raymond V, Dubois S, Malyukova I (2003) Gene expression profile of the human trabecular meshwork: NEIBank sequence tag analysis. *Invest Ophthalmol Vis Sci* 44: 2588–2596.
54. Xue W, Wallin R, Olmsted-Davis EA, Borrás T (2006) Matrix GLA protein function in human trabecular meshwork cells: inhibition of BMP2-induced calcification process. *Invest Ophthalmol Vis Sci* 47: 997–1007.
55. Junglas B, Yu AH, Welge-Lüssen U, Tamm ER, Fuchshofer R (2009) Connective tissue growth factor induces extracellular matrix deposition in human trabecular meshwork cells. *Exp Eye Res* 88: 1065–1075.
56. Balint E, Lapointe D, Drissi H, van der Meijden C, Young DW, et al. (2003) Phenotype discovery by gene expression profiling: mapping of biological processes linked to BMP-2-mediated osteoblast differentiation. *J Cell Biochem* 89: 401–426.
57. Diskin S, Kumar J, Cao Z, Schuman JS, Gilmartin T, et al. (2006) Detection of differentially expressed glycogenes in trabecular meshwork of eyes with primary open-angle glaucoma. *Invest Ophthalmol Vis Sci* 47: 1491–1499.
58. Vittal V, Rose A, Gregory KE, Kelley MJ, Acott TS (2005) Changes in gene expression by trabecular meshwork cells in response to mechanical stretching. *Invest Ophthalmol Vis Sci* 46: 2857–2868.
59. Zhao X, Ramsey KE, Stephan DA, Russell P (2004) Gene and protein expression changes in human trabecular meshwork cells treated with transforming growth factor-beta. *Invest Ophthalmol Vis Sci* 45: 4023–4034.
60. Tovar-Vidales T, Roque R, Clark AF, Wordinger RJ (2008) Tissue transglutaminase expression and activity in normal and glaucomatous human trabecular meshwork cells and tissues. *Invest Ophthalmol Vis Sci* 49: 622–628.
61. Jono S, Nishizawa Y, Shioi A, Morii H (1997) Parathyroid hormone-related peptide as a local regulator of vascular calcification. Its inhibitory action on in vitro calcification by bovine vascular smooth muscle cells. *Arterioscler Thromb Vasc Biol* 17: 1135–1142.
62. Rozsa FW, Reed DM, Scott KM, Pawar H, Moroi SE, et al. (2006) Gene expression profile of human trabecular meshwork cells in response to long-term dexamethasone exposure. *Mol Vis* 12: 125–141.
63. Filla MS, Liu X, Nguyen TD, Polansky JR, Brandt CR, et al. (2002) In vitro localization of TIGR/MYOC in trabecular meshwork extracellular matrix and binding to fibronectin. *Invest Ophthalmol Vis Sci* 43: 151–161.

64. Yorio T, Krishnamoorthy R, Prasanna G (2002) Endothelin: is it a contributor to glaucoma pathophysiology? *J Glaucoma* 11: 259–270.
65. Bradley JM, Vranka J, Colvis CM, Conger DM, Alexander JP, et al. (1998) Effect of matrix metalloproteinases activity on outflow in perfused human organ culture. *Invest Ophthalmol Vis Sci* 39: 2649–2658.
66. Buie L, Spiga M, Kennedy K, Fowler W, Borrás T (2010) Overexpression of MMP1 by an Adenoviral Vector (Ad) Hampers Myocilin (MYOC) Expression. *Invest Ophthalmol Vis Sci ARVO*: # 3222.
67. Fautsch MP, Vrabel AM, Peterson SL, Johnson DH (2004) In vitro and in vivo characterization of disulfide bond use in myocilin complex formation. *Mol Vis* 10: 417–425.
68. Mukaiyama H, Tohda H, Takegawa K (2010) Overexpression of protein disulfide isomerases enhances secretion of recombinant human transferrin in *Schizosaccharomyces pombe*. *Appl Microbiol Biotechnol* 86: 1135–1143.
69. Kleiner A, Shakhnovich E (2007) The mechanical unfolding of ubiquitin through all-atom Monte Carlo simulation with a Go-type potential. *Biophys J* 92: 2054–2061.
70. Yoo BC, Krapfenbauer K, Cairns N, Belay G, Bajo M, et al. (2002) Overexpressed protein disulfide isomerase in brains of patients with sporadic Creutzfeldt-Jakob disease. *Neurosci Lett* 334: 196–200.
71. Giannandrea M, Bianchi V, Mignogna ML, Sirri A, Carrabino S, et al. (2010) Mutations in the small GTPase gene RAB39B are responsible for X-linked mental retardation associated with autism, epilepsy, and macrocephaly. *Am J Hum Genet* 86: 185–195.
72. Zeiger W, Ito D, Swetlik C, Oh-Hora M, Villereal ML, et al. (2011) Stannocalcin 2 Is a Negative Modulator of Store-Operated Calcium Entry. *Mol Cell Biol* 31: 3710–3722.
73. Surgucheva I, Park BC, Yue BY, Tomarev S, Surguchov A (2005) Interaction of myocilin with gamma-synuclein affects its secretion and aggregation. *Cell Mol Neurobiol* 25: 1009–1033.
74. Giasson BI, Forman MS, Higuchi M, Golbe LI, Graves CL, et al. (2003) Initiation and synergistic fibrillization of tau and alpha-synuclein. *Science* 300: 636–640.
75. Eller M, Williams DR (2011) alpha-Synuclein in Parkinson disease and other neurodegenerative disorders. *Clin Chem Lab Med* 49: 403–408.
76. McKinnon SJ (2003) Glaucoma: ocular Alzheimer's disease? *Front Biosci* 8: s1140–s1156.
77. Hentze H, Lin XY, Choi MS, Porter AG (2003) Critical role for cathepsin B in mediating caspase-1-dependent interleukin-18 maturation and caspase-1-independent necrosis triggered by the microbial toxin nigericin. *Cell Death Differ* 10: 956–968.